

# **CROP TYPE MAPPING USING MULTITEMPORAL HYPERSPECTRAL IMAGES AND DEEP LEARNING**

YUCHIAN HUANG

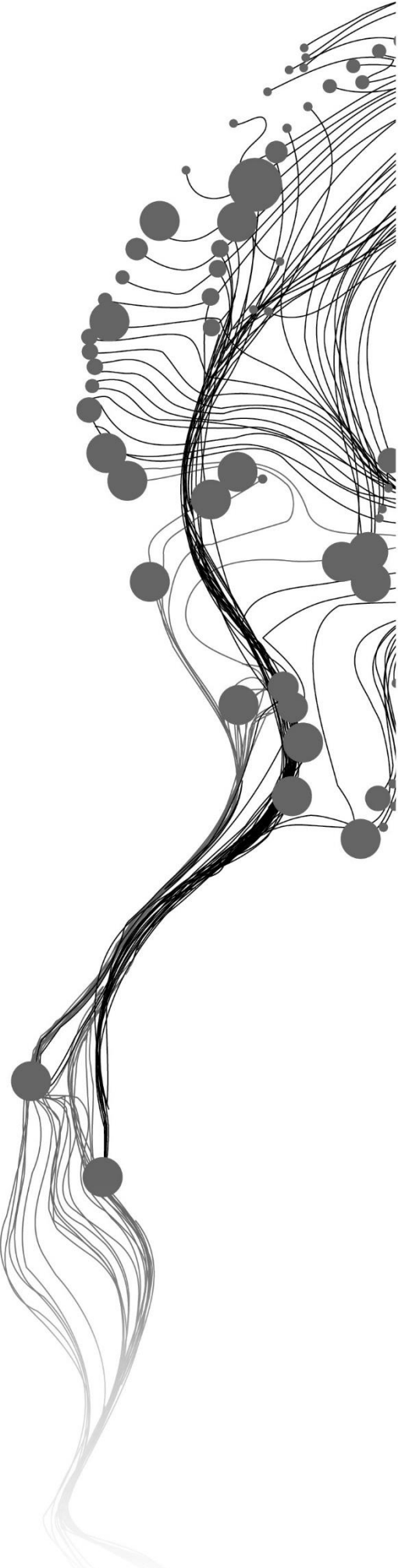
August, 2024

SUPERVISORS:

Dr. Ir. W. Bijker

Dr. M. Belgiu





# CROP TYPE MAPPING USING MULTITEMPORAL HYPERSENSPECTRAL IMAGES AND DEEP LEARNING

YUCHIAN HUANG

Enschede, The Netherlands, August, 2024

Thesis submitted to the Faculty of Geo-Information Science and Earth Observation of the University of Twente in partial fulfilment of the requirements for the degree of Master of Science in Geo-information Science and Earth Observation.

Specialization: Geoinformatics

**SUPERVISORS:**

Dr. Ir. W. Bijker

Dr. M. Belgiu

**THESIS ASSESSMENT BOARD:**

Prof. Dr. Ir. C. Persello (Chair)

Dr. Ir. T.A. Groen (External Examiner)

#### DISCLAIMER

This document describes work undertaken as part of a programme of study at the Faculty of Geo-Information Science and Earth Observation of the University of Twente. All views and opinions expressed therein remain the sole responsibility of the author, and do not necessarily represent those of the Faculty.

# ABSTRACT

This study investigates the application of hyperspectral imagery and deep learning techniques for crop type mapping. With global food security threatened by population growth and climate change, accurate crop type mapping becomes essential for estimating crop yields and optimizing agricultural management. Traditional methods using multispectral images face limitations in distinguishing crops with similar spectral characteristics. This research addresses these challenges by leveraging the high spectral resolution of hyperspectral imagery and the temporal analysis capabilities of deep learning models.

The study area in Belgium provided a diverse range of annual crops. Hyperspectral datasets from the PRISMA satellite and labeled training samples from the Flemish government were utilized to classify the different crops. Two deep learning models, 2D CNN for single-date imagery and 3D CNN for multi-temporal imagery, were developed and evaluated.

Results demonstrated that the 3D CNN model significantly improved classification accuracy by capturing the temporal dynamics of crop growth, achieving higher overall accuracy compared to the 2D CNN model. Most crops, including corn, “flax and hemp”, sugar beets, “grains, seeds and legumes”, and “vegetables, herbs, and ornamental plants”, exhibited improved classification performance with multi-temporal images compared to single-date images. However, for crops prone to classification ambiguity, such as grasslands and forages, the benefits of multi-temporal data are less pronounced. Early stopping techniques further enhanced the models' generalization capabilities, reducing overfitting. The findings explore the potential of integrating hyperspectral and multi-temporal data for precise crop classification, offering valuable insights for agricultural monitoring and management.

**Keywords:** Crop classification; Hyperspectral images; Multi-temporal analysis; Deep learning

# ACKNOWLEDGEMENTS

First and foremost, my deepest respect and gratitude go to my thesis supervisors, Dr. W. Bijker (Wietske) and Dr. M. Belgiu (Mariana), for their unwavering enthusiasm and support. They provided considerable expertise and many useful suggestions when I struggled with the problems in my progress of the thesis. Their dedication to high professional standards has been an invaluable source of inspiration.

I thank the members of my thesis assessment board: Prof. Dr. Ir. C. Persello (Claudio), Dr. Ir. T.A. Groen (Thomas), and Dr. C.M. Gevaert (Caroline). I am indebted to their feedback and advice. Also, I thank my thesis proposal and mid-term assessment board: Prof. Dr. Ir. A. Stein and Drs. J.P.G. Bakx. They gave me useful guidance and told me what I could do in the future research process.

I also like to extend my gratitude to individuals who collaborated and provided insightful expertise on my code: Kwasi Appiah-Gyimah Ofori-Karikari and Chenxi Duan. Their technical assistance was crucial in overcoming various challenges I encountered.

My daily routine was greatly enriched by my fellow students in ITC, including Alma Raunak, Faheed Jasin, Chakshu Gururani, Griija Sekar, Sergar Sari, Mahasen Kulugamma, Salsabila Prasetya, Maulana Ikram Wibisana, Varavarai Suwannapura, and TzuHsiang Lo. Thank you for helping me review my thesis draft and ask me some critical questions to stimulate my thinking. I also deeply enjoyed the friendship of my friends outside of ITC, especially Kaiyuan Hsu, Bangyu Lan, Yixiang Lu, and Chinying Lin. Without such friends, I couldn't finish my thesis efficiently.

Finally, I heartily thank my family for all their encouragement. They provided me the numerous funding sources that supported me finish my Master's degree in the Netherlands. Thank you for always believing in me to study abroad and pursue my goals.

# TABLE OF CONTENTS

---

1. Introduction .....	1
1.1. Background .....	1
1.2. Research objective and research questions .....	4
2. Study areas and datasets .....	5
2.1. Study area.....	5
2.2. Datasets .....	6
3. Research methods .....	8
3.1. Workflow .....	8
3.2. Pre-processing of hyperspectral imagery .....	9
3.3. Training sample preparation .....	12
3.4. Deep learning model .....	15
3.5. Accuracy assessment.....	19
3.6. Comparative analysis of single-date images and multi-temporal image .....	20
4. Results .....	21
4.1. Classification result before early stopping.....	21
4.2. Classification result after early stopping.....	27
5. Discussion.....	34
5.1. Evaluating the impact of early stopping on classification accuracies.....	34
5.2. Ambiguity of crop type classification results.....	35
5.3. Single-date image analysis.....	37
5.4. Multi-temporal image analysis and comparative evaluation .....	38
6. Conclusion.....	41
6.1. Answer to research questions.....	41
6.2. Conclusion.....	41
6.3. Research challenges .....	42
6.4. Future research direction.....	43
7. Ethical considerations, risks and contingencies .....	44
Annex 1. Wavelength range of merging bands on PRISMA imagery .....	51

## LIST OF FIGURES

---

Figure 1. Study area of this research .....	5
Figure 2. Workflow for evaluating and comparing the performance of 2D and 3D CNN models on single-date and multi-temporal PRISMA images, with and without early stopping, to determine the effectiveness of temporal information in image classification .....	8
Figure 3. Spatial representation of 6-meter buffer zones and crop type pixels .....	13
Figure 4. 2D CNN network architecture for single-date crop classification, where $h$ and $w$ represent the image height and width, respectively. The model employs $3 \times 3$ convolutions, adaptive max pooling, and FC layers (64 neurons, 8 output classes) .....	16
Figure 5. 3D CNN network architecture for multitemporal crop classification, where $n=3$ is the number of images, $w$ is the width, and $h$ is the height. The network utilizes multiple $3 \times 3 \times 3$ convolutions, adaptive max pooling, and FC layers for classification with 64 and $c$ (the number of classes=8) units respectively. ....	18



## LIST OF TABLES

---

Table 1. PRISMA PAN, VNIR, and SWIR bands and their wavelength ranges .....	6
Table 2. PRISMA acquisition dates and corresponding cloud cover of the selected images.....	7
Table 3. The dates and cloud cover for the target images (PRISMA) and reference images (Sentinel 2A) .....	11
Table 4. Training sample data in the study area.....	14
Table 5. Training and validation data sample sizes for the deep learning model.....	15
Table 6. Confusion matrix for April training sample classification before early stopping .....	22
Table 7. Confusion matrix for April validation sample classification before early stopping.....	22
Table 8. Confusion matrix for July training sample classification before early stopping.....	23
Table 9. Confusion matrix for July validation sample classification before early stopping .....	24
Table 10. Confusion matrix for August training sample classification before early stopping .....	25
Table 11. Confusion matrix for August validation sample classification before early stopping.....	25
Table 12. Confusion matrix for multi-temporal training sample classification before early stopping...	26
Table 13. Confusion matrix for multi-temporal validation sample classification before early stopping .....	27
Table 14. Confusion matrix for April training sample classification after early stopping .....	28
Table 15. Confusion matrix for April validation sample classification after early stopping .....	28
Table 16. Confusion matrix for July training sample classification after early stopping .....	29
Table 17. Confusion matrix for July validation sample classification after early stopping .....	30
Table 18. Confusion matrix for August training sample classification after early stopping .....	31
Table 19. Confusion matrix for August validation sample classification after early stopping .....	31
Table 20. Confusion matrix for multi-temporal training sample classification after early stopping.....	32
Table 21. Confusion matrix for multi-temporal validation sample classification after early stopping ..	33
Table 22. Comparison between classification accuracies before and after early stopping .....	35
Table 23. The individual crop classification accuracy improvements on validation data using early stopping .....	39

# 1. INTRODUCTION

## 1.1. Background

The main threats to global food security are world population growth and climate change. The world's population is expected to grow to 9.7 billion by 2050 (United Nations, 2019), while climate change is already causing more extreme weather events, such as droughts and floods. These combinations of factors are more likely to affect food supplies and quality. To address the problem, crop type mapping is applied to help governments estimate crop yields and predict the influence of climate change (Wang et al., 2023). Besides, accurate crop type mapping may enable governments to optimize land resources and agricultural management (Farmonov et al., 2023).

Remote sensing methods have been used for crop classification since the 1970s (Torbick et al., 2018). In this regard, multispectral images (e.g., Landsat, Sentinel 2, or SPOT images) are frequently applied to classify various crop types because multispectral data provides valuable information about the spectral properties and spatial patterns of different crop types. To be more specific, the spectral signatures of crops depend on factors such as plant health, plant pigments, leaf water content, and ground cover, and, consequently, each crop species has a unique spectral response (Zhang et al., 2020). Therefore, different crop types can be identified and classified by analyzing the spectral signatures of crops from multispectral images (Yi et al., 2020).

However, despite the advancements in multispectral images, the limited number of spectral bands in multispectral imagery cannot identify different crop types with similar spectral characteristics (Lu et al., 2020). For example, maize and soybeans have similar spectral signatures when using the limited number of bands in multispectral imagery, which may make it difficult to discriminate between these two crop types (Skakun et al., 2016). In contrast, hyperspectral imagery provides a much higher spectral resolution and detailed information across hundreds of contiguous, narrow spectral bands. It captures detailed spectral signatures of vegetation which are influenced by the biochemical and biophysical properties of each crop (Teke et al., 2013).

In addition, temporal information is also essential for distinguishing between different crop types in satellite imagery. Initially, the classification of individual crops relied on single-date images, but this approach may not be accurate because the same crop has a variety of growth patterns, development stages, and harvesting times on a particular date. It is difficult to identify specific crop types on the single-date satellite image. To overcome this challenge, multi-temporal images have been applied in crop type mapping. This is because multi-temporal images can capture every growth stage of the crops, and different crops with similar spectral signatures can be discriminated by tracking changes over time (Vuolo et al., 2018; Zhang et al., 2020). Although multi-temporal images improve classification accuracy, some crops are often confused with each other, i.e. high misclassification rate, due to their similar temporal profiles. For instance, corn and potato cannot be differentiated very well because of their similar growing cycles (Piedelobo et al., 2019).

In recent years, deep learning techniques have gained importance in crop type mapping using multi-temporal or hyperspectral datasets (Spiller et al., 2021; Zhang et al., 2020). One of the primary advantages of deep learning models in agriculture is their ability to handle multi-temporal datasets effectively (Li et al., 2023). Unlike traditional machine learning models, deep learning algorithms can automatically extract features through backpropagation during training, which is so suitable for dealing with multi-temporal images involving seasonal patterns (Wang et al., 2022). For example, three-dimensional CNN models can acquire temporal, spectral, and spatial information from the images simultaneously (Ji et al., 2018; Li et al., 2023). Additionally, deep learning models can effectively cope with hyperspectral remote sensing data (Khan et al., 2022). This is because deep learning algorithms can be used to reduce the dimensionality of the hyperspectral datasets which contain a large number of spectral bands, and extract spatial and spectral information from the image. This can lead to better accuracy of deep learning models on the remote sensing hyperspectral data (Bhosle & Musande, 2022).

Although the combination of deep learning techniques with multi-temporal hyperspectral imaging has great potential in crop classification, there are several challenges that hinder its widespread adoption of hyperspectral datasets. One challenge is the limited availability of training data. This is because hyperspectral images provide abundant information that contains a spectrum of hundreds of spectral bands for each pixel. This makes it difficult to find enough labeled training data to train the model that can generalize well to new data (Xie et al., 2023).

More importantly, limited research has explored the potential of crop type mapping using multi-temporal hyperspectral images and deep learning, with most studies focusing on a single hyperspectral image or multi-temporal multispectral images. Some studies used hyperspectral images and deep learning for crop classification, and they primarily focused on single hyperspectral images rather than incorporating images during the target crop growth cycle (Spiller et al., 2021; Xie et al., 2023). Other studies focused on crop classification using multitemporal multispectral images, and found that the temporal information might help deep learning models learn spatio-temporal features from remote sensing images (Ji et al., 2018; Li et al., 2023; Zhong et al., 2019).

Therefore, the focus of this study is to combine the advantages of abundant labeled sample datasets, hyperspectral images, multi-temporal datasets, and deep learning models on crop mapping. By leveraging the advantages of high spectral resolution of hyperspectral imagery and the feature extraction capabilities of deep learning, the research aims to explore the potential of multi-temporal hyperspectral image analysis for crop type mapping. Crucially, the inclusion of large numbers of samples is anticipated to address the challenges of generalization and overfitting identified in previous studies, ultimately contributing to improved multi-temporal crop-type maps with high precision.

## **1.2. Research objective and research questions**

### **1.2.1. Research objective**

The main objective of this research is to evaluate the impact of multi-temporal hyperspectral data on the accuracy and effectiveness of crop type mapping compared to single-date hyperspectral imagery, while applying deep learning techniques.

### **1.2.2. Research questions**

- a. How effectively can deep learning models extract discriminative features from single-date hyperspectral imagery to differentiate between crop types?
- b. What are the comparative performance and accuracy of single-date images and multi-temporal images in classifying different types of crops?

## 2. STUDY AREAS AND DATASETS

### 2.1. Study area

The study area is located in the West Flanders province of Belgium, specifically encompassing the regions of Diksmuide, Houthulst, and Lo-Reninge. The study area (red rectangle in Figure 1) has a length of 24 km, a width of 21 km, and covers an area of 504km<sup>2</sup> (Figure 1).

In general, lands are flat in this study area. Flat lands tend to have more uniform soil conditions and water distribution, which can lead to more consistent growth patterns among crops. Besides, The study area is primarily dominated by annual crops, which have distinct, predictable growth cycles within a single year. Most crops are planted in spring and are harvested in autumn. The features of this location make it a good study area for multi-temporal crop type mapping.

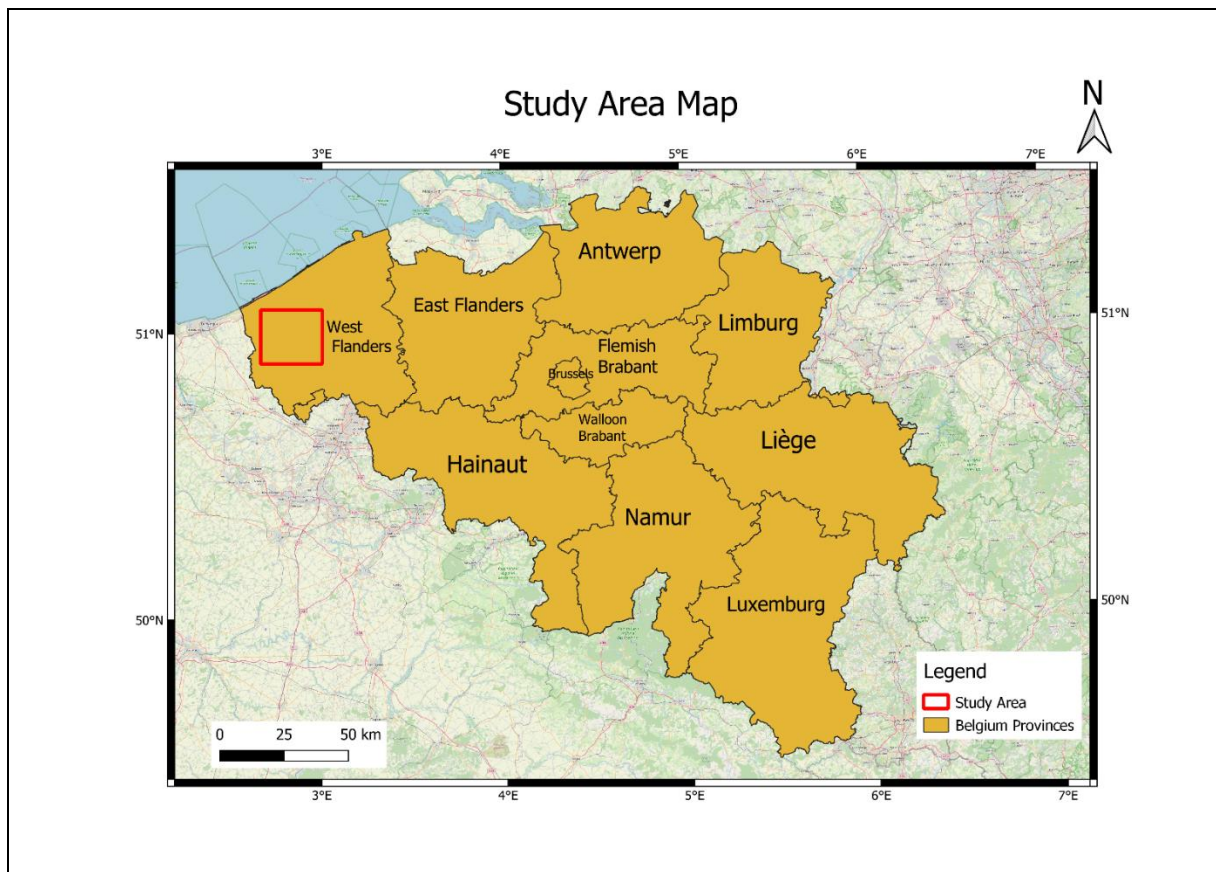


Figure 1. Study area of this research

## 2.2. Datasets

### 2.2.1. Hyperspectral satellite data

Hyperspectral datasets were downloaded from the PRISMA satellite website (<https://prismauserregistration.asi.it/>) and read using the “prismaread” R package (Busetto & Ranghetti, 2020). PRISMA is an Earth Observation satellite owned and operated by the Italian Space Agency (ASI). It was launched on March 22, 2019, and is designed to provide hyperspectral imagery of the Earth's surface. PRISMA has a total of 240 spectral and continuous bands ranging between 400 and 2500 nm. PRISMA's hyperspectral sensor has a spatial resolution of 30 meters (Shaik et al., 2023). Table 1 shows the description of the PRISMA image wavelength. This study uses VNIR and SWIR bands to classify crops without using the panchromatic band.

Table 1. PRISMA PAN, VNIR, and SWIR bands and their wavelength ranges

<b>Spectral range</b>	<b>Wavelength range</b>	<b>The Numbers of bands</b>	<b>Spatial resolution</b>
Visible near-infrared (VNIR)	400–1010 nm	66	30 m
Short-wave infrared (SWIR)	920–2500 nm	173	30 m
Panchromatic (PAN)	400–700 nm	1	5 m

In this research, Level 2D (L2D) PRISMA products were utilized to classify different crops. The choice of L2D products is due to their inclusion of reflectance values that are both geocoded and orthorectified (Delogu et al., 2023). The images were captured from the growing season of 2022 between March and October.

Cloud cover obstructs the view of the Earth's surface, and its presence in satellite images can affect their usability (Whitcraft et al., 2015). To ensure the clarity and usability of the images, only those with less than 1% cloud cover were selected for this study. Table 2. lists the acquisition dates and the percentage of cloud coverage for the images used in this research.

Table 2. PRISMA acquisition dates and corresponding cloud cover of the selected images

<b>Date</b>	<b>Cloud coverage (%)</b>
2022-04-16	0.06
2022-07-17	0.02
2022-08-09	0.02

### **2.2.2. Labeled data**

Labeled data was obtained from the Flander's government website (<https://www.geopunt.be/inspire>). This data includes the information on the main crop cultivated for all agricultural plots in Belgium, which was collected on April 21, 2022. The farmers supplied the information on the main crops they cultivated on their agricultural plots. The labeled data includes the following classes: 1. Corn, 2. Flax and Hemp, 3. Forages, 4. Fruit and nuts, 5. Grains, seeds, and legumes, 6. Grassland, 7. Other crops, 8. Sugar beets, 9. Potatoes, 10. Vegetables, herbs, and ornamental plants, 11. Woody plants.



## 3. RESEARCH METHODS

### 3.1. Workflow

The focus of this research is to advance crop classification accuracy and efficiency by synergizing available Prisma images collected across different times along the crop growing season and deep learning methodologies. To achieve the research objectives outlined above, a comprehensive research workflow has been designed (Figure 2). The phases of the research shown in Figure 2 will be described in the remainder of this chapter.

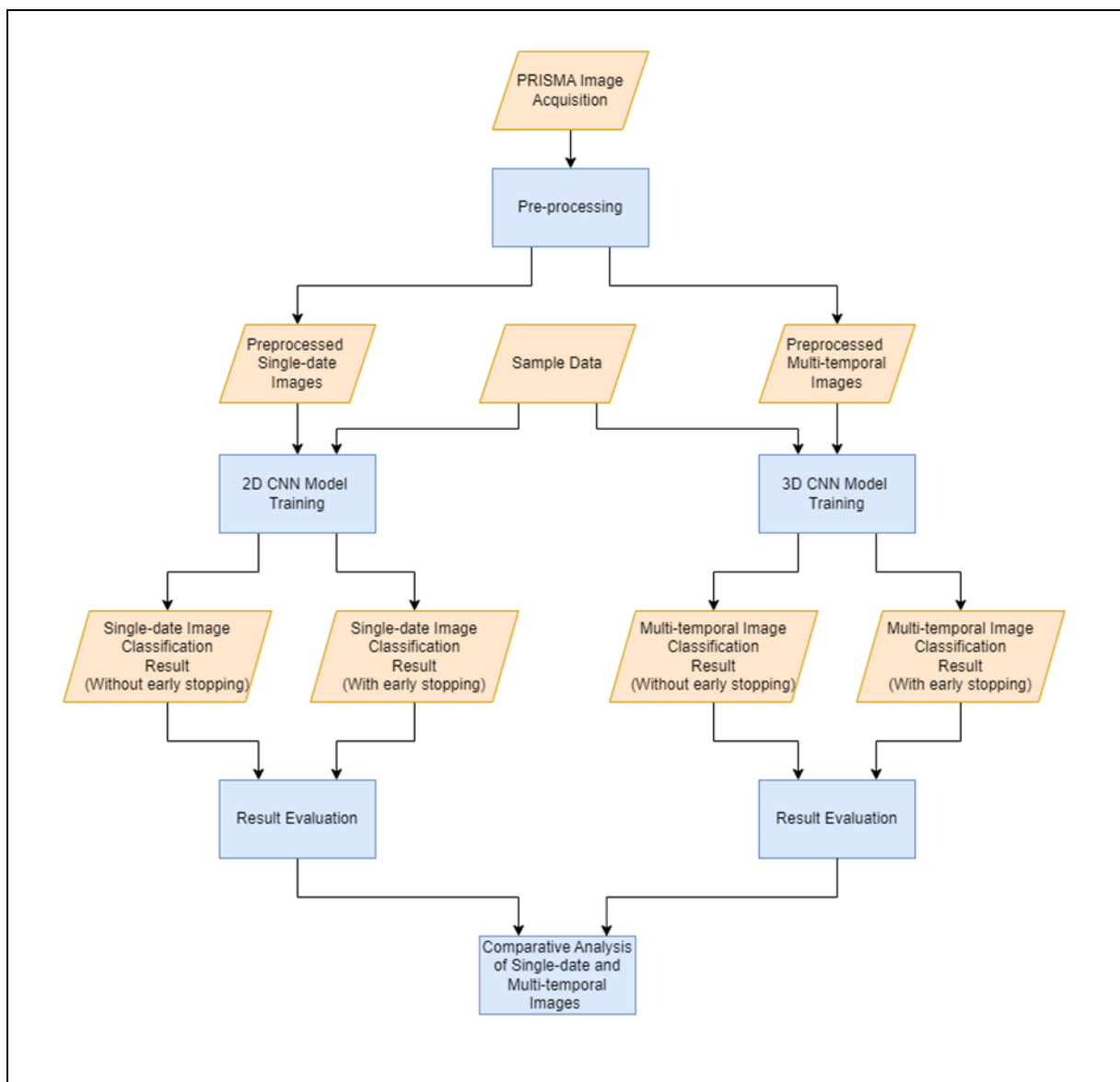


Figure 2. Workflow for evaluating and comparing the performance of 2D and 3D CNN models on single-date and multi-temporal PRISMA images, with and without early stopping, to determine the effectiveness of temporal information in image classification

## **3.2. Pre-processing of hyperspectral imagery**

Hyperspectral imagery was collected from the Prisma website. The dates of the image was chosen between March and October during the whole growing season. Then, although the PRISMA Products Specification Document claimed that the PRISMA images were orthorectified successfully, there were issues with line misalignments among different hyperspectral images, indicating a lack of standardized procedures for orienting them (Baiocchi et al., 2022). Therefore, PRISMA images were pre-processed to ensure data consistency, quality, and compatibility. This includes geometric correction and orthorectification (Lu et al., 2020).

### **3.2.1. Hyperspectral images type conversion**

The "prismaread" R package (Busetto & Ranghetti, 2020) facilitates the conversion of PRISMA hyperspectral data from the original ASI-provided HDF format to more manageable formats (GeoTIFF). PRISMA sensors record data in two spectral bands: VNIR (Visible and Near Infrared) and SWIR (Short Wave Infrared). These bands partially overlap; the VNIR band ranges from 400 nm to 975 nm, while the SWIR band spans from 939 nm to 2500 nm, creating an overlap between 939 nm and 975 nm.

To address potential redundancy or confusion during data conversion or analysis due to this overlap, the "prismaread" package includes a `join_priority` setting. This setting allows users to specify which band's data should be prioritized in the overlapping range. By setting the priority to "SWIR," the data from the SWIR band is preferentially used for the wavelengths between 939 nm and 975 nm. This functionality ensures clear and effective management of spectral data where the VNIR and SWIR bands intersect. After merging the bands using this approach, the hyperspectral data is consolidated into 230 bands, reducing redundancy and simplifying subsequent analysis. Annex 1. shows the wavelength range before merging bands and after merging bands.

### 3.2.2. Coregistration of hyperspectral images

To fix misaligned PRISMA data, AROSICS (Python package) was used to perform automatic subpixel co-registration of two satellite image datasets based on image matching (Scheffler et al., 2017).

AROSICS (Automated and Robust Open-Source Image Co-Registration Software) is a Python-based software designed for automatic sub-pixel co-registration of multi-sensor data based on image matching. The primary goal was to ensure that a target image matches a reference image as closely as possible in terms of geographical position and alignment. The process of the algorithm was divided into three steps: input data preparation, detection of geometric shifts, and correction of displacements.

Firstly, because the numbers of bands of a target image and a reference image might be different, spectral bands from different images had to be selected for image matching. If the co-registration was achieved using the selected bands, the same transformation (shifts and alignments) could be applied to the other bands of a target image. Secondly, the algorithm used grids of points to identify corresponding points or features on overlapping areas of the target and reference images and estimate X/Y offsets on both images. The final step involved correcting the detected displacements to align the target image with the reference image accurately. Affine transformation was applied to ensure the reliability and accuracy of subpixel co-registration.

In this study, PRISMA images were defined as the target image, and the Sentinel 2A images were used as the reference image. Sentinel 2 images have been proven to be effective reference images for the co-registration process of PRISMA data, thereby improving the quality of PRISMA data (De Luca et al., 2024). Table 3. shows the dates and cloud cover percentage on the target images and reference images. The assumption of this algorithm was to correspond the wavelength range of band 51 (843.87 nm - 854.59 nm) of PRISMA images to that of band 8 of the Sentinel 2A images (NIR band, 785 nm - 900 nm) first. After determining the geometric correction parameters (shift vectors, rotation angles) from band 51 of the PRISMA images, these parameters could be applied to all other bands of the PRISMA image. In addition, the parts of images that include the ocean were omitted in this process because water lacks fixed

reference points, making it nearly impossible to obtain consistent measurements (Román et al., 2024).

Table 3. The dates and cloud cover for the target images (PRISMA) and reference images (Sentinel 2A)

<b>Target images</b>		<b>Reference images</b>	
<b>PRISMA images (Spatial Resolution: 30m)</b>		<b>Sentinel 2A images (Spatial Resolution: 10m)</b>	
<b>Time</b>	<b>Cloud coverage (%)</b>	<b>Time</b>	<b>Cloud coverage (%)</b>
2022-04-16	0.06	2022-04-20	18.79
2022-07-17	0.02	2022-07-19	0.08
2022-08-09	0.02	2022-08-11	0.05

### 3.2.3. Hyperspectral image resampling

Pixel grids from different images could not align with each other because three PRISMA images were captured from different angles. To overcome this issue, a cubic spline resampling method was utilized to align the pixels with each other. This method leveraged cubic convolution, which utilizes 16 pixels to compute an output pixel value. The April Image was chosen as the reference, with July and August images being resampled to match its spatial resolution and alignment. Although the cloud cover in April was slightly higher than in July and August, it remains very low (0.06%). The April image, taken before large-scale crop growth, minimized the impact of vegetation growth and seasonal changes on image alignment.

### **3.3. Training sample preparation**

#### **3.3.1. Labeled dataset reprojection**

Labeled crop data was acquired from the Vlaams government website. The labeled dataset was projected in Belge 1972 / Belgian Lambert 72 (EPSG:31370), and hyperspectral images were projected in WGS 84 / UTM zone 31N (EPSG:32631). The coordination systems are different on these types of datasets. To transform from one coordinate system to another, the labeled dataset was reprojected in WGS 84 / UTM zone 31N (EPSG:32631).

#### **3.3.2. Feature matching**

To accurately identify pixels of interest, the initial step involved creating pixels on the labeled data that correspond to the satellite imagery (the grid size: 30m). This alignment enabled the precise extraction of pixels within the designated polygon areas, ensuring that the pixels in the labeled data accurately match those in the satellite imagery (Li et al., 2020; Siesto et al., 2021). Subsequently, a 6-meter buffer was generated around the boundaries of a field to avoid edge effects. These edge effects often result from a mixture of different crops and the presence of features like fences, ditches, and uncropped areas, which do not accurately reflect the actual crop types from the labeled data. By creating a buffer, these edge effects could be excluded, ensuring that the data collected from within the buffer represents the field's interior conditions more accurately. Figure 3 shows the boundaries of the crop fields, buffer zones, and selected crop pixels. Because of the consideration of the Hughes phenomenon, some crop types were excluded in Figure 3. The detailed information was described in the chapter 3.3.3.



Figure 3. Spatial representation of 6-meter buffer zones and crop type pixels

### 3.3.3. Selection of training and validation samples

From the overall labeled dataset, 800 pixels from each crop type were randomly selected as the sample data. These pixels were further divided into two independent sets: the training sample set (560 pixels), and the validation sample set (240 pixels), thereby maintaining a 7:3 ratio. The key approach was to ensure that training and validation pixels were selected from different agricultural plots. Table 4 shows the numbers of agricultural plots and corresponding pixels in the study area. This separation guarantees that the training and validation datasets are independent and do not overlap, effectively preventing overfitting.

Another crucial consideration was that the number of training and validation samples should exceed the number of spectral bands to avoid the Hughes phenomenon. The Hughes phenomenon, also known as the curse of dimensionality, occurs when the number of spectral bands (features) is very high compared to the number of training samples, which leads to a decrease in classification accuracy (Pal & Foody, 2010). In this study, the number of spectral bands was effectively reduced to 230 after merging some of bands, which ensured that the number of training and validation samples exceeds the number of spectral bands.

In this study, certain classes such as Woody plants and Other crops were constrained by having fewer than 230 valid pixels (Table 4). 230 is the number of spectral bands of the satellite data. This insufficient sample size hindered the feasibility of running a deep learning model effectively. Additionally, Fruit and nuts was excluded from the study. This is because the available data could not guarantee that training and validation pixels were selected from different agricultural plots if more than 230 valid pixels were extracted. Consequently, eight classes were selected for the study to adapt to this constraint and ensure robust model training. Table 5 shows the number of training and validation samples per class for the deep learning model.

Table 4. Training sample data in the study area

<b>Class (Dutch)</b>	<b>Class (English)</b>	<b>The total of pixels</b>	<b>The total of agricultural plots</b>	<b>Choice</b>
Aardappelen	Potatoes	21014	1593	Yes
Fruit en Noten	Fruit and Nuts	613	72	No
Granen, zaden en peulvruchten	Grains, seeds and legumes	27961	1853	Yes
Grasland	Grassland	40741	4881	Yes
Groenten, kruiden en sierplanten	Vegetables, herbs and ornamental plants	17669	1349	Yes
Houtachtige gewassen	Woody plants	15	6	No
Maïs	Corn	38075	3586	Yes
Overige gewassen	Other crops	181	48	No
Suikerbieten	Sugar beets	6634	382	Yes
Vlas en hennep	Flax and hemp	1457	87	Yes
Voedergewassen	Forages	4410	391	Yes

Table 5. Training and validation data sample sizes for the deep learning model

Class	Training Samples (Pixels)	Validation Samples (Pixels)
Corn	560	240
Forages	560	240
Flax and hemp	560	240
Grains, seeds and legumes	560	240
Grassland	560	240
Potatoes	560	240
Sugar beets	560	240
Vegetables, herbs and ornamental plants	560	240
Total	4480	1920

### 3.4. Deep learning model

A CNN model was used in this research due to its ability to handle high-dimensional data. This is because hyperspectral images contain a large number of spectral bands. CNN can capture the correlations between different spectral bands while integrating spatial information (Guerra et al., 2023). Additionally, CNN excels at learning distinctive spatio-temporal features of crops from the remote sensing data (Ji et al., 2018).

The 2D CNN model can extract spectral and spatial features within pre-processed hyperspectral images simultaneously (Vaddi & Manoharan, 2020), and the 3D CNN model can incorporate temporal features from hyperspectral images, capturing unique spectral signatures, temporal variations in crop growth, and crop spatial distribution within the imagery. (Ji et al., 2018).



### 3.4.1. 2D CNN structure for single-date hyperspectral image classification

The 2D CNN model was used to classify crops using a single-date hyperspectral image. The model leverages a sequential layer structure. The input data is represented as 2D tensors with spectral and spatial dimensions ( $230, n, w$ ). Here, 230 corresponds to the number of bands in the PRISMA data after merging, and  $h$  and  $w$  represent the image height and width, respectively. These tensors are processed through three convolutional layers. Each convolutional layer is followed by a ReLU activation and adaptive max-pooling operations, aimed at capturing both spectral and spatial features essential for accurate crop classification (Ji et al., 2018; Seyrek & Uysal, 2024; Zafar et al., 2022). Specifically, the first convolutional layer utilizes 32 kernels, the second layer uses 64 kernels, and the third layer employs 128 kernels, each with a  $3 \times 3$  kernel size to extract multi-level features from the input data. The final feature maps are then flattened and passed through fully connected (FC) layers, which consist of 64 neurons before outputting predictions across 8 crop classes. The 2D CNN network structure is shown in Figure 4. This model employed a constant learning rate of 0.0005 and utilized a batch size of 8. The default epoch size is 300.

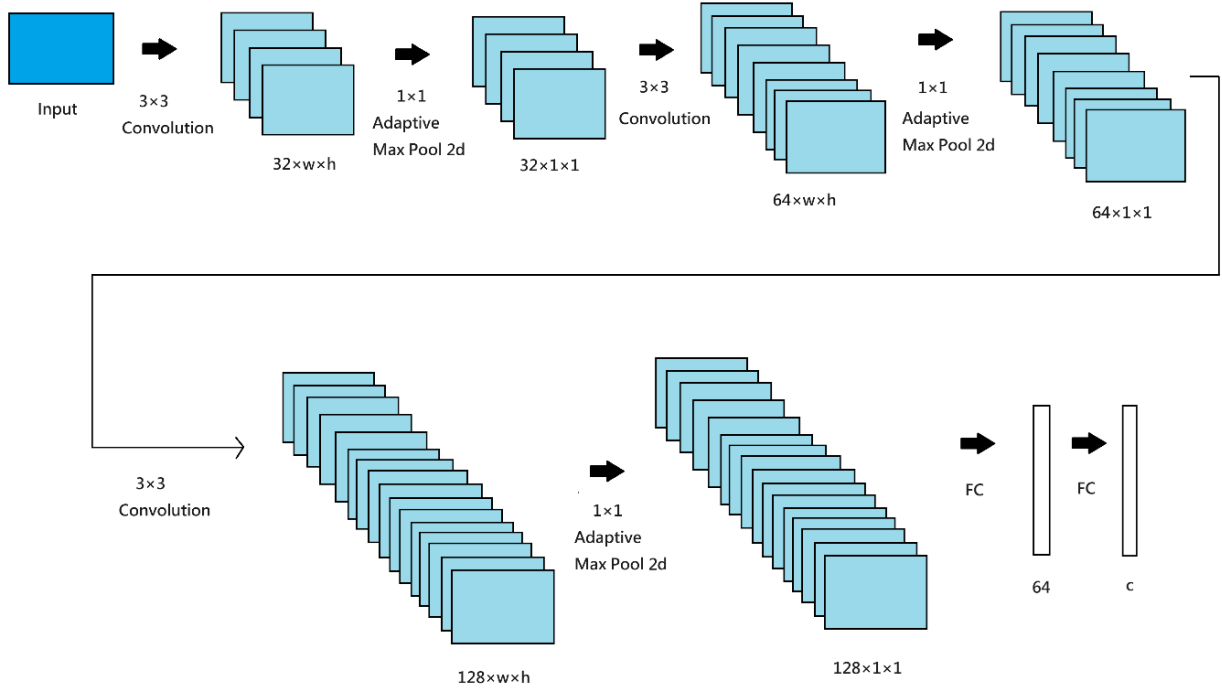


Figure 4. 2D CNN network architecture for single-date crop classification, where  $h$  and  $w$  represent the image height and width, respectively. The model employs  $3 \times 3$  convolutions, adaptive max pooling, and FC layers (64 neurons, 8 output classes).

### 3.4.2. 3D CNN structure for multi-temporal hyperspectral image classification

The 3D CNN was used to process multi-temporal satellite data. The input data was represented as 3D tensors with spectral, spatial, and temporal dimensions  $(230, n, w, h)$ , where 230 is the number of spectral bands in the PRISMA data after merging,  $w$  represents the image width,  $h$  represents the image height, and  $n$  represents the number of images in the time dimension ( $n=3$ ).

The network architecture comprised three convolutional layers followed by FC layers, as depicted in Figure 5. Each convolutional layer used a kernel size of  $3 \times 3 \times 3$ , with the number of kernels increasing sequentially through the layers: 32, 64, and 128, respectively. These layers extract spatial-temporal features from the input data, which consist of multi-band satellite images over three time periods.

To preserve temporal information until the final classification stage, an applied adaptive max pooling was applied in each convolutional layer, ensuring that the temporal dimension remains uncompressed until reaching the FC layers. The FC layers consist of 64 neurons in the first layer and output neurons corresponding to the number of classes ( $c=8$ ) in the final layer. The network structure is shown in Figure 5. The Adam optimizer was chosen due to its demonstrated superiority over other stochastic optimization methods. Its effectiveness has been validated in various multi-temporal classification (H. Zhao et al., 2019). The fixed learning rate is 0.0005 and the batch size is 8. The default epoch size is 300.

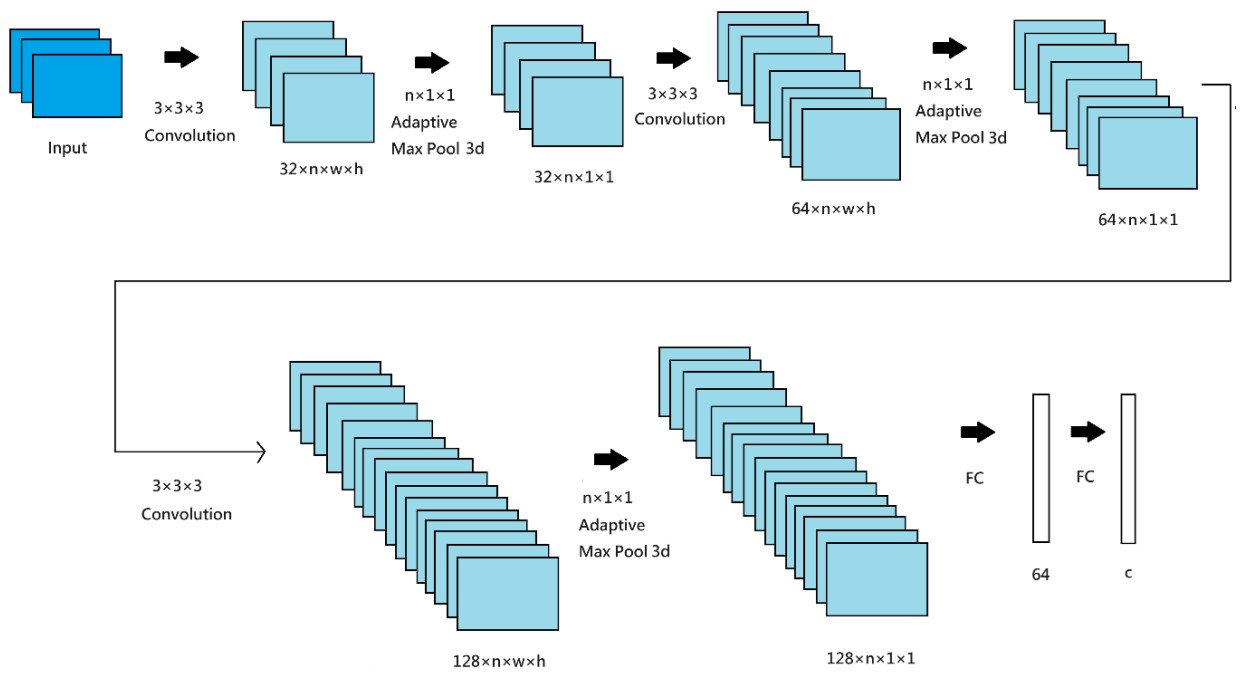


Figure 5. 3D CNN network architecture for multitemporal crop classification, where  $n=3$  is the number of images,  $w$  is the width, and  $h$  is the height. The network utilizes multiple  $3 \times 3 \times 3$  convolutions, adaptive max pooling, and FC layers for classification with 64 and  $c$  (the number of classes=8) units respectively.

### 3.4.3. Early stopping technique

To evaluate the performance of a deep learning model, it will be trained both without early stopping and with early stopping. Initially, the model will be trained without using early stopping to establish its baseline performance. This approach allows observation of the model's behavior when it is allowed to train for the full number of epochs without interruption, helping to identify any potential overfitting issues.

Early stopping is a technique used in training machine learning models to prevent overfitting and improve generalization. Overfitting occurs when a model learns the training data too well, capturing noise and fluctuations, which reduces its performance on new, unseen data. Early stopping involves monitoring the model's performance on a validation set during training. If the validation performance starts to deteriorate while training performance continues to improve, it

signals overfitting. Training is stopped at the point where the validation performance is best, which typically corresponds to the model being more generalized and robust (Lu et al., 2022).

The categorical cross-entropy loss function, which integrates cross-entropy loss with a softmax activation, was employed for this study. This function is particularly effective for multi-class classification tasks, such as crop type mapping (T. Lu et al., 2022; Mohammadi et al., 2021; H. Zhao et al., 2019). The function is defined mathematically as shown in Equation:

$$CrossEntropyLoss = \sum_{c=1}^M y_{o,c} \log(p_{o,c})$$

Where:

$M$  is the number of classes.

$y_{o,c}$  is a binary indicator (0 or 1) if class label  $c$  is the correct classification for observation  $o$ .

$p_{o,c}$  is the predicted probability that observation  $c$ .

Additionally, a patience parameter of 10 epochs is implemented to mitigate the risk of overfitting. This parameter operates under the principle that if the validation loss ceases to decrease over a span of 10 consecutive epochs, it indicates that the model may be starting to learn noise and irrelevant details from the training dataset.

Therefore, in Chapter 4.1, the model will be trained without early stopping to establish baseline performance. In Chapter 4.2, early stopping techniques will be applied to classify the crops. This approach is expected to provide insights into the model's performance both without and with early stopping.

### 3.5. Accuracy assessment

To evaluate the results, accuracy assessments, such as a confusion matrix, are employed to evaluate the model's performance in correctly identifying crop types (Niu et al., 2022). The confusion matrix helps to extract accuracy metrics like overall accuracy (OA), user accuracy (UA), and producer accuracy (PA). Misclassified crop types are analyzed alongside accuracy assessments by comparing them with sample data from the government to determine the causes of misclassification.

### **3.6. Comparative analysis of single-date images and multi-temporal image**

To further assess the performance of the crop type mapping framework, a comparative analysis was conducted using both single-date images and a multi-temporal image. For the single-date image analysis, models trained on hyperspectral images from specific months (April, July, August) are analyzed to assess their performance. This evaluation focuses on the OA from each image and examines the individual crop type performance based on UA and PA.

For the multi-temporal image analysis, the study employed a 3D CNN model to analyze both spatial, spectral, and temporal features, providing insights into the OA for each result and how the OA improves compared to the single-date image's OA. This comparison aims to determine the differences in classification accuracy between the single-date images (April, July, and August) versus multi-temporal datasets.

## 4. RESULTS

This chapter discusses the performance of crop classification models using both single-date and multi-temporal satellite images. The analysis focuses on the comparison of the classification results for various crops, both before and after the implementation of early stopping. This comparison aims to know the impact of the model performance with early stopping and without early stopping.

### 4.1. Classification result before early stopping

#### 4.1.1. Single-date Image Classification Result

Table 6. and Table 7. show the confusion matrices for April's training and validation classifications. In the training sample classification, the model achieved an OA of 67%. “Grains, seeds, and legumes” performed best, with 88% UA and 93% PA. Corn had a UA of 47% and a PA of 44%. For the validation sample classification, the OA dropped to 52%, with Corn at 39% UA and 25% PA, and “Grains, seeds, and legumes” at 80% UA and 87% PA. In brief, this result indicates varying performance, with the highest accuracy in “grains, seeds, and legumes” and the lowest in corn and “vegetables, herbs, and ornamental plants”.

Table 6. Confusion matrix for April training sample classification before early stopping

	Corn	Flax and hemp	Forages	Grains, seeds, and legumes	Grassland	Potatoes	Sugar beets	Vegetables, herbs, and ornamental plants	Total	UA (%)
<b>Corn</b>	271	46	27	6	12	118	40	62	582	47%
<b>Flax and hemp</b>	12	519	0	8	0	16	2	6	563	92%
<b>Forages</b>	64	5	289	4	86	14	3	10	475	61%
<b>Grains, seeds, and legumes</b>	17	8	8	479	31	2	0	1	546	88%
<b>Grassland</b>	44	2	94	3	432	0	0	1	576	75%
<b>Potatoes</b>	71	19	14	6	6	332	36	67	551	60%
<b>Sugar beets</b>	21	108	16	1	0	61	365	12	584	63%
<b>Vegetables, herbs, and ornamental plants</b>	111	7	5	7	5	131	23	274	563	49%
<b>Total</b>	611	714	453	514	572	674	469	433	4440	
<b>PA (%)</b>	44%	73%	64%	93%	76%	49%	77%	63%	<b>OA (%)</b>	<b>67%</b>

Table 7. Confusion matrix for April validation sample classification before early stopping

	Corn	Flax and hemp	Forages	Grains, seeds, and legumes	Grassland	Potatoes	Sugar beets	Vegetables, herbs, and ornamental plants	Total	UA (%)
<b>Corn</b>	85	17	10	5	4	49	13	35	218	39%
<b>Flax and hemp</b>	31	127	0	4	0	31	35	9	237	54%
<b>Forages</b>	71	8	144	3	69	23	6	1	325	44%
<b>Grains, seeds, and legumes</b>	18	4	4	202	17	2	2	5	254	80%
<b>Grassland</b>	23	0	35	2	163	1	0	0	224	73%
<b>Potatoes</b>	35	6	7	9	1	122	20	49	249	49%
<b>Sugar beets</b>	16	37	5	2	0	43	91	22	216	42%
<b>Vegetables, herbs, and ornamental plants</b>	60	16	3	4	2	55	18	79	237	33%
<b>Total</b>	339	215	208	231	256	326	185	200	1960	
<b>PA (%)</b>	25%	59%	69%	87%	64%	37%	49%	40%	<b>OA (%)</b>	<b>52%</b>

Table 8. and Table 9. reveal the confusion matrices for July's training and validation sample classifications, with an OA of 88% in training and 81% in validation. Corn shows strong accuracy with 96% UA and 91% PA in training, and 93% UA and 84% PA in validation. “Flax and hemp” performs similarly well, with 97% UA and 96% PA in training, and 90% UA and 94% PA in validation. Sugar beets excel with 98% UA in both sets. However, forages and grassland show lower accuracies.

Table 8. Confusion matrix for July training sample classification before early stopping

	Corn	Flax and hemp	Forages	Grains, seeds, and legumes	Grassland	Potatoes	Sugar beets	Vegetables, herbs, and ornamental plants	Total	UA (%)
Corn	558	3	1	1	1	4	0	14	582	96%
Flax and hemp	1	545	0	17	0	0	0	0	563	97%
Forages	6	0	323	1	72	8	64	1	475	68%
Grains, seeds, and legumes	0	12	2	525	1	0	0	6	546	96%
Grassland	4	6	171	5	381	1	0	8	576	66%
Potatoes	20	0	11	0	1	487	14	18	551	88%
Sugar beets	2	0	0	0	0	7	572	3	584	98%
Vegetables, herbs, and ornamental plants	20	0	0	0	0	23	0	520	563	92%
Total	611	566	508	549	456	530	650	570	4440	
PA (%)	91%	96%	64%	96%	84%	92%	88%	91%	<b>OA (%)</b>	<b>88%</b>



Table 9. Confusion matrix for July validation sample classification before early stopping

	Corn	Flax and hemp	Forages	Grains, seeds, and legumes	Grassland	Potatoes	Sugar beets	Vegetables, herbs, and ornamental plants	Total	UA (%)
Corn	202	1	0	0	2	0	2	11	218	93%
Flax and hemp	4	213	0	20	0	0	0	0	237	90%
Forages	7	0	154	1	85	9	62	7	325	47%
Grains, seeds, and legumes	2	10	2	231	3	1	0	5	254	91%
Grassland	1	1	64	3	153	2	0	0	224	68%
Potatoes	13	0	7	0	0	215	8	6	249	86%
Sugar beets	0	0	1	2	0	1	211	1	216	98%
Vegetables, herbs, and ornamental plants	12	2	0	7	0	4	1	211	237	89%
Total	241	227	228	264	243	232	284	241	1960	
PA (%)	84%	94%	68%	88%	63%	93%	74%	88%	<b>OA (%)</b>	<b>81%</b>

Table 10. and Table 11. demonstrate the confusion matrices for August's training and validation sample classifications across various crops. The training set shows an OA of 90%, with corn achieving 98% UA and 96% PA. “Flax and hemp” also performs well with 99% UA and PA. In contrast, forages have a lower UA of 50% and PA of 81%. Validation results show an OA of 80%, with corn at 94% UA and 93% PA, and flax and hemp at 92% UA and 95% PA. Forages remain low with 30% UA and 73% PA. The results highlight the model's strengths in correctly classifying corn, “flax and hemp”, and sugar beets, but indicate room for improvement in forages and “vegetables, herbs, and ornamental plants”.

Table 10. Confusion matrix for August training sample classification before early stopping

	Corn	Flax and hemp	Forages	Grains, seeds, and legumes	Grassland	Potatoes	Sugar beets	Vegetables, herbs, and ornamental plants	Total	UA (%)
Corn	571	0	1	1	0	8	0	1	582	98%
Flax and hemp	0	560	0	1	0	2	0	0	563	99%
Forages	6	1	237	0	169	4	58	0	475	50%
Grains, seeds, and legumes	2	5	1	520	2	12	0	4	546	95%
Grassland	0	1	49	8	511	2	0	5	576	89%
Potatoes	3	0	0	5	0	537	1	5	551	97%
Sugar beets	3	0	3	0	0	1	575	2	584	98%
Vegetables, herbs, and ornamental plants	10	0	0	4	0	51	0	498	563	88%
Total	595	567	291	539	682	617	634	515	4440	
PA (%)	96%	99%	81%	96%	75%	87%	91%	97%	OA (%)	90%

Table 11. Confusion matrix for August validation sample classification before early stopping

	Corn	Flax and hemp	Forages	Grains, seeds, and legumes	Grassland	Potatoes	Sugar beets	Vegetables, herbs, and ornamental plants	Total	UA (%)
Corn	205	0	1	0	0	6	2	4	218	94%
Flax and hemp	0	219	0	8	3	5	0	2	237	92%
Forages	5	0	97	0	153	9	59	2	325	30%
Grains, seeds, and legumes	2	11	1	222	2	10	0	6	254	87%
Grassland	2	0	31	3	185	2	0	1	224	83%
Potatoes	5	0	0	4	0	229	2	9	249	92%
Sugar beets	1	0	2	0	2	0	209	2	216	97%
Vegetables, herbs, and ornamental plants	1	0	0	11	0	30	5	190	237	80%
Total	221	230	132	248	345	291	277	216	1960	
PA (%)	93%	95%	73%	90%	54%	79%	75%	88%	OA (%)	80%

#### 4.1.2. Multi-temporal Image Classification Result

Table 12. and Table 13. depict the confusion matrices for multi-temporal training and validation sample classifications. In the training set, the OA is 96%. Corn achieved 99% UA and 98% PA. “Flax and hemp”, “grains, seeds, and legumes”, sugar beets, and “vegetables, herbs, and ornamental plants” all achieved 100% UA and PA. Validation results show an OA of 85%, with corn at 94% UA and 88% PA, and “flax and hemp’ at 96% UA and 95% PA. Forages had lower accuracy, with 54% UA and 78% PA. These results highlight strong performance in most crops, with some improvement needed in forages and grassland.

Table 12. Confusion matrix for multi-temporal training sample classification before early stopping

	Corn	Flax and hemp	Forages	Grains, seeds, and legumes	Grassland	Potatoes	Sugar beets	Vegetables, herbs, and ornamental plants	Total	UA (%)
Corn	578	0	0	0	0	1	0	3	582	99%
Flax and hemp	0	563	0	0	0	0	0	0	563	100%
Forages	0	0	409	0	23	0	43	0	475	86%
Grains, seeds, and legumes	0	0	0	546	0	0	0	0	546	100%
Grassland	0	0	75	0	498	0	0	3	576	86%
Potatoes	10	2	0	0	0	528	1	10	551	96%
Sugar beets	0	0	1	0	0	0	583	0	584	100%
Vegetables, herbs, and ornamental plants	0	0	0	0	0	1	0	562	563	100%
Total	588	565	485	546	521	530	627	578	4440	
PA (%)	98%	100%	84%	100%	96%	100%	93%	97%	OA (%)	96%

Table 13. Confusion matrix for multi-temporal validation sample classification before early stopping

	Corn	Flax and hemp	Forages	Grains, seeds, and legumes	Grassland	Potatoes	Sugar beets	Vegetables, herbs, and ornamental plants	Total	UA (%)
Corn	204	0	1	0	0	4	1	8	218	94%
Flax and hemp	0	228	0	9	0	0	0	0	237	96%
Forages	6	0	177	0	93	0	38	11	325	54%
Grains, seeds, and legumes	1	9	1	238	1	0	0	4	254	94%
Grassland	2	1	43	2	176	0	0	0	224	79%
Potatoes	14	0	1	0	1	217	3	13	249	87%
Sugar beets	1	0	4	0	0	0	207	4	216	96%
Vegetables, herbs, and ornamental plants	4	2	0	6	1	10	3	211	237	89%
Total	232	240	227	255	272	231	252	251	1960	
PA (%)	88%	95%	78%	93%	65%	94%	82%	84%	<b>OA (%)</b>	85%

## 4.2. Classification result after early stopping

### 4.2.1. Single-date Image Classification Result

Table 14 and Table 15 display the confusion matrices for the April images with early stopping for both training and validation samples across various agricultural classes. Early stopping was applied at epoch 37, with a final training loss of 1.1956 and validation loss of 1.4378. The OA achieved with early stopping is 54% for the training samples and 48% for the validation samples. To be more specific, "Flax and hemp" demonstrates a high UA of 85% and PA of 86% in the training set but drops to 60% UA and 59% PA in the validation set. Classes like corn and "vegetables, herbs and ornamental plants" show notably low accuracies, indicating challenges in correctly classifying these categories.

Table 14. Confusion matrix for April training sample classification after early stopping

	Corn	Flax and hemp	Forages	Grains, seeds, and legumes	Grassland	Potatoes	Sugar beets	Vegetables, herbs, and ornamental plants	Total	UA (%)
Corn	9	75	104	14	79	140	94	67	582	2%
Flax and hemp	3	476	1	5	0	33	39	6	563	85%
Forages	5	9	253	3	155	23	16	11	475	53%
Grains, seeds, and legumes	1	10	56	435	31	2	2	9	546	80%
Grassland	0	1	152	16	402	0	1	4	576	70%
Potatoes	6	34	9	4	7	316	110	65	551	57%
Sugar beets	0	121	4	0	2	89	362	6	584	62%
Vegetables, herbs, and ornamental plants	9	23	25	26	52	242	57	129	563	23%
Total	33	749	604	503	728	845	681	297	4440	
PA (%)	27%	64%	42%	86%	55%	37%	53%	43%	OA (%)	54%

Table 15. Confusion matrix for April validation sample classification after early stopping

	Corn	Flax and hemp	Forages	Grains, seeds, and legumes	Grassland	Potatoes	Sugar beets	Vegetables, herbs, and ornamental plants	Total	UA (%)
Corn	5	22	32	6	41	54	27	31	218	2%
Flax and hemp	0	142	0	0	0	42	50	3	237	60%
Forages	1	7	127	3	133	27	16	11	325	39%
Grains, seeds, and legumes	0	12	33	182	21	0	3	3	254	72%
Grassland	0	1	48	5	170	0	0	0	224	76%
Potatoes	2	17	3	3	5	134	50	35	249	54%
Sugar beets	1	51	0	0	2	33	120	9	216	56%
Vegetables, herbs, and ornamental plants	1	24	8	18	21	79	34	52	237	22%
Total	10	276	251	217	393	369	300	144	1960	
PA (%)	50%	51%	51%	84%	43%	36%	40%	36%	OA (%)	48%

The confusion matrices for July (Table 16. & Table 17.) illustrate the classification performance with early stopping at epoch 58, where the training loss was 0.3897 and the validation loss was 0.5456. The OA achieved was 85% for training and 80% for validation samples. UA were notably high for many classes, with "Corn" achieving 92% in training and 91% in validation, and "Potatoes" reaching 95% in both training and validation. However, the "Forages" and "Grassland" categories demonstrated more crucial classification challenges. "Forages" had a UA of 42% in training and 36% in validation, indicating difficulties in correctly classifying this category. PA for "Forages" was 62% in training and 73% in validation, showing some improvement but still lower than other classes.

Table 16. Confusion matrix for July training sample classification after early stopping

	Corn	Flax and hemp	Forages	Grains, seeds, and legumes	Grassland	Potatoes	Sugar beets	Vegetables, herbs, and ornamental plants	Total	UA (%)
Corn	538	4	4	1	0	24	0	11	582	92%
Flax and hemp	1	535	0	27	0	0	0	0	563	95%
Forages	8	0	200	2	181	22	61	1	475	42%
Grains, seeds, and legumes	0	24	2	508	1	1	4	6	546	93%
Grassland	1	1	112	14	437	3	0	8	576	76%
Potatoes	8	0	4	1	1	525	1	11	551	95%
Sugar beets	3	0	1	0	0	16	559	5	584	96%
Vegetables, herbs, and ornamental plants	14	0	0	5	0	47	16	481	563	85%
Total	573	564	323	558	620	638	641	523	4440	
PA (%)	94%	95 %	62 %	91%	70%	82%	87%	92%	<b>OA (%)</b>	<b>85%</b>

Table 17. Confusion matrix for July validation sample classification after early stopping

	Corn	Flax and hemp	Forages	Grains, seeds, and legumes	Grassland	Potatoes	Sugar beets	Vegetables, herbs, and ornamental plants	Total	UA (%)
Corn	198	1	2	1	1	4	0	11	218	91%
Flax and hemp	9	195	0	33	0	0	0	0	237	82%
Forages	6	1	116	1	121	18	56	6	325	36%
Grains, seeds, and legumes	0	20	2	225	1	2	0	4	254	89%
Grassland	0	1	38	3	180	2	0	0	224	80%
Potatoes	5	0	2	0	1	237	1	3	249	95%
Sugar beets	1	0	0	1	0	5	209	0	216	97%
Vegetables, herbs, and ornamental plants	7	6	0	4	0	14	8	198	237	84%
Total	226	224	160	268	304	282	274	222	1960	
PA (%)	88%	87%	73%	84%	59%	84%	76%	89%	<b>OA (%)</b>	<b>80%</b>

The confusion matrices for August (Table 18. and Table 19.) detail the classification performance with early stopping, reflecting results for both training and validation samples. These results were obtained after early stopping at epoch 66. The training sample achieved an OA of 81%, while the validation sample reached an OA of 73%. UA was notably high for several categories: "Corn" achieved a 95% UA in training and 90% in validation, while "Potatoes" reached 90% UA in training and 86% in validation. These high accuracies indicate a strong performance in correctly classifying these crops.

However, the "Forages" category faced serious challenges, with a UA of only 22% in training and 20% in validation. This low accuracy suggests difficulties in distinguishing "Forages" from other categories. The PA for "Forages" was also relatively low, at 62% in training and 50% in validation, further emphasizing the need for improvement in this category's classification.

Table 18. Confusion matrix for August training sample classification after early stopping

	Corn	Flax and hemp	Forages	Grains, seeds, and legumes	Grassland	Potatoes	Sugar beets	Vegetables, herbs, and ornamental plants	Total	UA (%)
Corn	552	0	6	1	1	15	0	7	582	95%
Flax and hemp	2	538	3	14	6	0	0	0	563	96%
Forages	11	5	104	0	277	9	68	1	475	22%
Grains, seeds, and legumes	4	35	0	457	12	33	1	4	546	84%
Grassland	1	6	49	10	503	0	0	7	576	87%
Potatoes	13	0	7	10	0	498	6	17	551	90%
Sugar beets	5	0	0	0	0	13	563	3	584	96%
Vegetables, herbs, and ornamental plants	31	0	0	8	0	95	35	394	563	70%
Total	619	584	169	500	799	663	673	433	4440	
PA (%)	89%	92%	62%	91%	63%	75%	84%	91%	<b>OA (%)</b>	<b>81%</b>

Table 19. Confusion matrix for August validation sample classification after early stopping

	Corn	Flax and hemp	Forages	Grains, seeds, and legumes	Grassland	Potatoes	Sugar beets	Vegetables, herbs, and ornamental plants	Total	UA (%)
Corn	196	0	4	0	0	11	0	7	218	90%
Flax and hemp	0	201	0	22	12	2	0	0	237	85%
Forages	7	0	66	0	179	8	64	1	325	20%
Grains, seeds, and legumes	2	23	4	201	4	16	0	4	254	79%
Grassland	2	1	21	5	195	0	0	0	224	87%
Potatoes	18	0	1	4	1	215	1	9	249	86%
Sugar beets	4	0	0	0	0	2	205	5	216	95%
Vegetables, herbs, and ornamental plants	7	0	0	10	0	39	24	157	237	66%
Total	236	225	96	242	391	293	294	183	1960	
PA (%)	83%	89%	69%	83%	50%	73%	70%	86%	<b>OA (%)</b>	<b>73%</b>



#### 4.2.2. Multi-temporal Image Classification Result

Table 20. and Table 21. demonstrate the confusion matrices for the multi-temporal training and validation sample classifications with early stopping. The confusion matrices for the multi-temporal training and validation sample classifications show robust model performance. The training set achieved an OA of 91%. Corn had 98% UA and 97% PA. “Flax and hemp” achieved 100% UA and PA, while forages had 51% UA and 75% PA. Validation results show an OA of 84%, with corn at 94% UA and 92% PA, and ‘flax and hemp’ at 98% UA and 96% PA. Forages had lower performance with 39% UA and 78% PA. The results indicate strong performance in most crops, with improvements needed for forages.

Table 20. Confusion matrix for multi-temporal training sample classification after early stopping

	Corn	Flax and hemp	Forages	Grains, seeds, and legumes	Grassland	Potatoes	Sugar beets	Vegetables, herbs, and ornamental plants	Total	UA (%)
Corn	568	0	1	0	1	3	0	9	582	98%
Flax and hemp	0	562	0	0	0	1	0	0	563	100%
Forages	2	0	240	0	177	2	51	3	475	51%
Grains, seeds, and legumes	1	3	0	525	10	1	3	3	546	96%
Grassland	1	0	74	2	491	0	0	8	576	85%
Potatoes	6	0	3	0	0	519	2	21	551	94%
Sugar beets	3	0	1	0	0	0	580	0	584	99%
Vegetables, herbs, and ornamental plants	5	0	0	3	0	16	6	533	563	95%
Total	586	565	319	530	679	542	642	577	4440	
PA (%)	97%	99%	75%	99%	72%	96%	90%	92%	<b>OA (%)</b>	<b>91%</b>

Table 21. Confusion matrix for multi-temporal validation sample classification after early stopping

	Corn	Flax and hemp	Forages	Grains, seeds, and legumes	Grassland	Potatoes	Sugar beets	Vegetables, herbs, and ornamental plants	Total	UA (%)
Corn	204	0	1	0	0	4	0	9	218	94%
Flax and hemp	0	233	0	1	3	0	0	0	237	98%
Forages	5	0	127	3	137	2	51	0	325	39%
Grains, seeds, and legumes	1	8	2	237	1	1	0	4	254	93%
Grassland	0	1	30	0	192	1	0	0	224	86%
Potatoes	7	0	2	0	0	232	1	7	249	93%
Sugar beets	0	0	1	0	0	1	214	0	216	99%
Vegetables, herbs, and ornamental plants	4	0	0	6	0	8	4	215	237	91%
Total	221	242	163	247	333	249	270	235	1960	
PA (%)	92 %	96%	78%	96 %	58%	93%	79 %	91%	<b>OA (%)</b>	<b>84%</b>

## 5. DISCUSSION

### 5.1. Evaluating the impact of early stopping on classification accuracies

Table 22. compares classification accuracies before and after early stopping for different datasets and model configurations. A noticeable gap between training and validation accuracies in the data before early stopping demonstrates overfitting. The results from the crop classification using single-date and multi-temporal images show a discrepancy between training and validation accuracy. For example, in the CNN2D model for April image classification, the training accuracy is 67% while the validation accuracy is only 52%. Similarly, in the multi-temporal image classification, the OA on the training set is 96%, higher than the OA on the validation set (85%). This large gap suggests that the model performs well on the training data but does not generalize effectively to unseen data.

In response to this challenge, chapter 4.2 explores the application of early stopping techniques to improve the model's generalization capabilities. Early stopping monitors the model's performance on a validation set and halts training once the performance ceases to improve, thus preventing the model from overfitting the training data. After implementing the early stopping techniques, the training accuracy becomes closer to the validation accuracy in each case. For example, April's training accuracy adjusts to 54% from 67%, and the validation accuracy becomes 48% from 52%, narrowing the gap to 6%. In multi-temporal classification, training accuracy adjusted from 96% to 91% and validation accuracy from 85% to 84%. Consequently, the gap between the training and validation accuracies narrowed from 11% to 7%. The decrease in the discrepancy between training and validation accuracies demonstrates an improvement in the model's generalization.

Table 22. Comparison between classification accuracies before and after early stopping

	<b>Training Samples Before Early Stopping</b>	<b>Validation Samples Before Early Stopping</b>	<b>Training Samples After Early Stopping</b>	<b>Validation Samples After Early Stopping</b>
<b>CNN2D-April</b>	67%	52%	54%	48%
<b>CNN2D-July</b>	88%	81%	85%	79%
<b>CNN2D-August</b>	90%	79%	81%	73%
<b>CNN3D-Multi- temporal</b>	96%	85%	91%	84%

## 5.2. Ambiguity of crop type classification results

### 5.2.1. The ambiguity between forages and grasslands

According to the confusion matrices in Chapter 4, grassland and forages display the lowest accuracies among the crops, especially in validation settings. The primary reason for this ambiguity is the overlap between these two classes.

Based on the sample data from the government, forages which include annual alfalfa, grass-clover mixes, grass-lucerne combinations, perennial alfalfa, mixtures of legumes, and mixed cultivation of maize and legume cultivation, as well as fodder beets. Forages is primarily grown and harvested to feed livestock (Capstaff & Miller, 2018). They are characterized by their cultivation and management for optimal nutritional content, yield, and palatability to ensure high-quality feed for animals.

In contrast, grasslands include sown grass seeds and permanent grassland areas on the basis of the sample data. These areas are often used for grazing livestock directly and are managed to maintain their ecological balance, biodiversity, and soil health (Fraser et al., 2022). Grasslands can be natural or semi-natural habitats that provide a range of ecosystem services beyond just forage production, such as carbon sequestration, water regulation, and habitat for wildlife (Zhao et al., 2020).

The ambiguity between forages and grasslands arises because both are used to feed livestock. Grasslands can serve as a source of forage either through direct grazing by animals or by being harvested for hay (Schils et al., 2022). This overlap in usage, along with the presence of grasses in both systems, complicates classification. Therefore, the result in this study is consistent with the previous studies because remote sensing images can't clearly differentiate between forages and grassland (Eder et al., 2023; Frank et al., 2022).

### **5.2.2. The ambiguity between sugar beets and forages**

There was a noticeable distinction between UA and PA in the context of classifying sugar beets, based on the confusion matrices of the sugar beets.

On one hand, UA for sugar beets was relatively good, which suggests that when the classification model can predict a pixel as sugar beet. This could be due to specific spectral signatures of sugar beets that the model learned to recognize well, making it effective at identifying pixels that are indeed sugar beets.

On the other hand, PA for sugar beets was not as good as UA. The relatively lower PA indicated that many pixels representing actual sugar beets were not being correctly classified as such by the model. Based on the labeled data from the government, fodder beets are categorized into the forage type because it is for the consumption of the livestock. However, fodder beets is still a kind of sugar beets per se (Evans & Messerschmidt, 2017; Wiśniewska et al., 2019). Therefore, there is ambiguity between sugar beets and forages in the result.

### 5.3. Single-date image analysis

The data reveals that crop classification accuracy fluctuates significantly throughout the year, aligning with the phenological stages of crop development. This variation is particularly pronounced when comparing the early season (April) to the peak growth months (July and August).

April presents substantial challenges for crop classification, largely due to the non-germinated state of many crops, and only bare soil being visible in many fields. The CNN 2D model shows significantly lower accuracy in April. When applying early stopping, the CNN 2D model shows a high increase in accuracy for April. For instance, the UA for corn is only 2% for both training and validation, with an OA of 54%. This issue is even more pronounced for “vegetables, herbs, and ornamental plants”, where UA is 23% in training and 22% in validation, with OAs of 54% and 48%, respectively. These results illustrate the difficulty of identifying crops that have barely started to grow.

Conversely, the classification accuracies increase considerably as the crops are fully developed and their distinct features become clearly visible. For example, with early stopping, corn’s UA in July is a robust 92% in training and 91% in validation. Sugar beets also display strong performance with a UA of 96% in training during July, reinforcing the advantage of later-season classification when the crops are fully developed. The OAs for these periods are impressive as well, with 85% in training and 79% in validation for July and an increase to 81% in training and 73% in validation by August.

These results confirm the findings of previous studies that demonstrate the challenge of crop classification in the early growing season. Maponya et al. (2020) and Veloso et al. (2017) used machine learning methods and Sentinel 2 images to classify different crops, comparing the performance between all single-date images. Accuracies during the early stages of crop development were low but improved dramatically as the growing season progressed and crops matured. This enhanced accuracy is attributed to the physical characteristics of the crops, such as distinct plant shapes, sizes, and the presence of mature plant features (Yi et al., 2020). In this study, crop type mapping using hyperspectral images and deep learning method showed similar

results, with lower classification accuracy from the April image compared to the July and August images.

To sum up, this analysis underlines the importance of considering the growth stage and the phenological characteristics of crops when deploying agricultural monitoring, as classification accuracy improves significantly as crops mature.

#### **5.4. Multi-temporal image analysis and comparative evaluation**

The utilization of 3D convolutional neural networks (3D CNN) in classifying crop types via hyperspectral imaging underscores the model's capacity to effectively capture the temporal dynamics of crop growth. The effective classification of “flax and hemp”, sugar beets, “vegetables, herbs, and ornamental plants”, as well as corn over time (as evidenced by high UA and PA percentages), suggests that the 3D CNN captures the temporal dynamics of crop growth well. This is important since these dynamics involve changes in spectral signatures as the crops grow, which are captured by the hyperspectral images. For instance, with early stopping, “flax and hemp” achieve a PA of 96% and a UA of 98%, while sugar beets impress with both PA and UA at 99% on the validation data. Similarly, “vegetables, herbs, and ornamental plants” registers 91% in both PA and UA, and corn show 92% and 94% in PA and UA respectively.

To evaluate the comparative performance and accuracy of single-date images versus multi-temporal images in crop classification, it is crucial to rely on validation and early stopping data. This approach ensures that the assessment of the models' effectiveness is based on their ability to generalize well to unseen data and prevents overfitting. The following analysis will utilize validation and early stopping data to delve into the specific performance outcomes of the use of single-date images and multi-temporal images.

In the analysis of existing outcomes, the evidence clearly shows that multi-temporal imaging outperform single-date imaging in crop classification. In both training and validation, 3D CNN models show at least a 4-5% increase in classification accuracy over 2D CNN model (Table 23), which might demonstrate the benefits of multi-temporal data. The finding is similar to the earlier research that compared crop classification accuracy between 2D and 3D CNN models

using Sentinel-2 imagery (Ji et al., 2018). They emphasized that OA of 3D CNN surpasses that of 2D CNN by roughly 3% on average.

Table 23. presents a comparison of the PA and UA improvements from single-time images to multi-temporal images for various crops. The columns include the highest UA and PA achieved with single-time images, the UA and PA achieved with multi-temporal images, and the respective improvements in accuracy. By selecting the highest UA and PA from single-time images, the analysis ensures that the most accurate single-time performance is compared with the multi-temporal performance. If multi-temporal imagery shows improvements over these best-case single-time results, it demonstrates the added value of temporal data.

Table 23. The individual crop classification accuracy improvements on validation data using early stopping

<b>Crop</b>	<b>Highest Single-Time UA</b>	<b>Highest Single-Time PA</b>	<b>Multi-temporal UA</b>	<b>Multi-temporal PA</b>	<b>UA Improvement</b>	<b>PA Improvement</b>
Corn	91%	88%	94%	92%	+3%	+4%
Flax and Hemp	82%	89%	98%	96%	+16%	+7%
Forages	39%	73%	39%	78%	0%	+5%
Grains, Seeds, and Legumes	89%	84%	93%	96%	+4%	+12%
Grasslands	87%	59%	86%	58%	-1%	-1%
Potatoes	95%	84%	93%	93%	-2%	+9%
Sugar Beets	97%	76%	99%	79%	+2%	+3%
Vegetables, Herbs, and Ornamental Plants	84%	89%	91%	79%	+7%	+2%

The use of multi-temporal imagery significantly enhances crop classification accuracy by capturing growth patterns and phenological changes over time. 3D CNN models are particularly effective in capturing these seasonal growth changes. Crops undergo distinct transitions from one growth phase to another, and accurately capturing these transitions is crucial for precise classification. Single-date images often depict fields as bare soil, especially in early spring,



posing classification challenges. However, crops like corn, “flax and hemp”, potatoes, sugar beets, and “vegetables, herbs, and ornamental plants”, which primarily grow in the summer, show improved classification accuracy when temporal data is utilized. For example, compared to the highest UA and PA from single-time images, corn's UA and PA increased by 3% and 4%, respectively, with the inclusion of multi-temporal data. Similarly, crops such as “grains, seeds, and legumes”, which grow between April and August, show marked accuracy improvements due to the detailed observation of their growth transitions, with UA and PA improvements of 4% and 12%, respectively.

However, the multi-temporal approach of 3D CNN models cannot enhance classification accuracy for crops with a high amount of misclassification, like grasslands and forages. These crops are hard to distinguish in single-date images, and even with the integration of multiple temporal data points, the improvements are minimal. For instance, grasslands show a slight decrease in both UA and PA by 1%, indicating the limitations of this approach for certain crop types.

In summary, multi-temporal imagery can enhance OA by capturing growth patterns and phenological changes efficiently. This method is especially beneficial for crops with overlapping spectral signatures and seasonal growth changes, leading to more precise agricultural monitoring. However, for certain crops like grasslands and forages, 3D CNN models can't show the improvements by integrating temporal data and hyperspectral imagery, demonstrating the limitations of this approach for certain crop types.

## 6. CONCLUSION

### 6.1. Answer to research questions

#### **RQ a. How effectively can deep learning models extract discriminative features from single-date hyperspectral imagery to differentiate between crop types?**

Deep learning models, particularly 2D CNN, can effectively extract discriminative features from single-date hyperspectral imagery to differentiate between crop types, but their effectiveness is highly influenced by the timing of the imagery. The models perform best when crops are fully developed and distinct features are visible, as seen in the improved accuracies during July and August.

#### **RQ b. What are the comparative performance and accuracy of single-date images and multi-temporal images in classifying different crop types?**

Multi-temporal images improve crop classification accuracy compared to single-date images. The OA from multi-temporal images outperforms the OA from the single-date images, with improvements in UA and PA for various crops. Besides, multi-temporal images improve most crops' PA and OA, such as corn, “flax and hemp”, sugar beets, “grains, seeds, and legumes” and “vegetables, herbs, and ornamental plants”. This enhancement is attributed to the models' ability to capture temporal changes and growth patterns, which are not available in single-date imagery. However, for crops such as grasslands and forages, which are prone to ambiguity, the advantages of multi-temporal data are minimal.

### 6.2. Conclusion

This research aims to integrate hyperspectral and multi-temporal imagery for the classification of different crops. The analysis indicates that the 3D CNN model, which utilizes multi-temporal hyperspectral imaging, outperforms single-date hyperspectral imaging in terms of crop classification accuracy. Most individual crops (corn, “flax and hemp”, sugar beets, “grains, seeds, and legumes” and “vegetables, herbs, and ornamental plants”, demonstrate better performance when using multi-temporal images compared to single-date images. Therefore,

multi-temporal hyperspectral imaging technology presents a valuable option for agricultural researchers who are striving for precision in crop monitoring and management. However, for crops prone to ambiguity, such as grasslands and forages, the benefits are not clear.

Besides, the findings from this research can contribute to Monitoring Agricultural ResourceS (MARS) project (European Commission, 2023). This project aims to provide timely and reliable information on crop conditions and yields across Europe. This study can help the project improve classification accuracy and calculate sown areas for different crop types throughout their growing seasons. This enhances yield predictions and provides insights of each crop growth stage, contributing to more effective agricultural resource management and planning (van der Velde & Nisini, 2019; Wu et al., 2023).

### **6.3. Research challenges**

There are several challenges of this research. Firstly, the findings may not be generalizable to other PRISMA datasets from different areas or times. To be more specific, PRISMA image acquisition is based on user demand, requiring users to specify the target areas beforehand (Vangi et al., 2021). Consequently, only three suitable PRISMA images are available for the study area and period covered in this research, as there are no other multi-temporal data available on the PRISMA website.

Another challenge in crop classification using hyperspectral images is the limited availability of data, particularly in the temporal dimension. This is because deep learning models rely on a diverse and extensive dataset to learn spectral, spatial, and temporal features effectively (Li et al., 2023). However, due to the absence of continuous multi-temporal data across the growing season, the ability of these models might not fully leverage temporal variations for distinguishing between different crop types.

#### **6.4. Future research direction**

This study establishes an initial foundation by comparing single-date and multi-temporal analysis to delineate the benefits of incorporating temporal data. Future work will extend this understanding by comparing the performance of multitemporal hyperspectral and multispectral data. By doing so, the impact of hyperspectral information on classification accuracy, particularly in relation to the spectral signature, can be better understood. This comparative analysis aims to identify the specific advantages and limitations of hyperspectral data over multispectral data in multi-temporal crop classification applications. By understanding these differences, it will be possible to achieve more precise and reliable classification outcomes.

Another future research direction involves comparing different machine learning and deep learning methods to determine the most effective approach for multitemporal crop type classification using hyperspectral imagery. This comparison will help identify the best techniques for utilizing the extensive data provided by hyperspectral imagery and multi-temporal analysis, further improving the precision and reliability of crop mapping.

## 7. ETHICAL CONSIDERATIONS, RISKS AND CONTINGENCIES

This research focused on the potential for image classification using deep learning algorithms. The algorithm was trained on a large dataset of images and used to identify crops in images. The research had a number of ethical implications, which needed to be addressed.

- Privacy and data security:

The data from Flemish government is anonymized and publicly available. The data has been stored on the University of Twente's OneDrive and used in this thesis.

- Citation practices:

All references were properly cited to avoid plagiarism and acknowledge previous work.

- The use of AI:

During the preparation of this work, ChatGPT was used to know the background knowledge if I couldn't understand the details of the previous papers. Grammarly helped me to correct the grammatical mistakes in my article. After using this tool, the content was reviewed and edited as needed, and I am fully responsible for the published content.

## LIST OF REFERENCES

---

- Baiocchi, V., Giannone, F., & Monti, F. (2022). How to orient and orthorectify PRISMA images and related issues. *Remote Sensing*, *14*(9). <https://doi.org/10.3390/rs14091991>
- Bhosle, K., & Musande, V. (2022). Evaluation of CNN model by comparing with convolutional autoencoder and deep neural network for crop classification on hyperspectral imagery. *Geocarto International*, *37*(3). <https://doi.org/10.1080/10106049.2020.1740950>
- Busetto, L., & Ranghetti, L. (2020). *prismaread: A tool for facilitating access and analysis of PRISMA L1/L2 hyperspectral imagery v1.0.0.*
- Capstaff, N. M., & Miller, A. J. (2018). Improving the yield and nutritional quality of forage crops. In *Frontiers in Plant Science* (Vol. 9). <https://doi.org/10.3389/fpls.2018.00535>
- De Luca, G., Carotenuto, F., Genesio, L., Pepe, M., Toscano, P., Boschetti, M., Miglietta, F., & Gioli, B. (2024). Improving PRISMA hyperspectral spatial resolution and geolocation by using Sentinel-2: development and test of an operational procedure in urban and rural areas. *ISPRS Journal of Photogrammetry and Remote Sensing*, *215*, 112–135. <https://doi.org/10.1016/j.isprsjprs.2024.07.003>
- Delogu, G., Caputi, E., Perretta, M., Ripa, M. N., & Boccia, L. (2023). Using PRISMA hyperspectral data for land cover classification with artificial intelligence support. *Sustainability (Switzerland)*, *15*(18). <https://doi.org/10.3390/su151813786>
- Eder, E., Riegler-Nurscher, P., Prankl, J., & Prankl, H. (2023). Grassland yield estimation using transfer learning from remote sensing data. *KI - Kunstliche Intelligenz*, *37*(2–4). <https://doi.org/10.1007/s13218-023-00814-9>
- European Commission. (2023). *Monitoring Agricultural ResourceS (MARS)*. [https://joint-research-centre.ec.europa.eu/monitoring-agricultural-resources-mars\\_en](https://joint-research-centre.ec.europa.eu/monitoring-agricultural-resources-mars_en)
- Evans, E., & Messerschmidt, U. (2017). Review: Sugar beets as a substitute for grain for lactating dairy cattle. In *Journal of Animal Science and Biotechnology* (Vol. 8, Issue 1). <https://doi.org/10.1186/s40104-017-0154-8>
- Farmonov, N., Amankulova, K., Szatmari, J., Sharifi, A., Abbasi-Moghadam, D., Mirhoseini Nejad, S. M., & Mucsi, L. (2023). Crop type classification by DESIS hyperspectral imagery and machine learning algorithms. *IEEE Journal of Selected Topics in Applied Earth Observations and Remote Sensing*, *16*, 1576–1588. <https://doi.org/10.1109/JSTARS.2023.3239756>

- Frank, T., Smith, A., Houston, B., Lindsay, E., & Guo, X. (2022). Differentiation of six grassland/forage types in three Canadian ecoregions based on spectral characteristics. *Remote Sensing*, *14*(9). <https://doi.org/10.3390/rs14092121>
- Fraser, M. D., Vallin, H. E., & Roberts, B. P. (2022). Animal board invited review: Grassland-based livestock farming and biodiversity. In *Animal* (Vol. 16, Issue 12). <https://doi.org/10.1016/j.animal.2022.100671>
- Guerri, M. F., Distante, C., Spagnolo, P., Bougourzi, F., & Taleb-Ahmed, A. (2023). *Deep learning techniques for hyperspectral image analysis in agriculture: a review*. <http://arxiv.org/abs/2304.13880>
- Ji, S., Zhang, C., Xu, A., Shi, Y., & Duan, Y. (2018). 3D convolutional neural networks for crop classification with multi-temporal remote sensing images. *Remote Sensing*, *10*(1). <https://doi.org/10.3390/rs10010075>
- Khan, A., Vibhute, A. D., Mali, S., & Patil, C. H. (2022). A systematic review on hyperspectral imaging technology with a machine and deep learning methodology for agricultural applications. In *Ecological Informatics* (Vol. 69). <https://doi.org/10.1016/j.ecoinf.2022.101678>
- Li, Q., Tian, J., & Tian, Q. (2023). Deep learning application for crop classification via multi-temporal remote sensing images. *Agriculture (Switzerland)*, *13*(4). <https://doi.org/10.3390/agriculture13040906>
- Li, Z., Chen, G., & Zhang, T. (2020). A CNN-Transformer hybrid approach for crop classification using multitemporal multisensor Images. *IEEE Journal of Selected Topics in Applied Earth Observations and Remote Sensing*, *13*. <https://doi.org/10.1109/JSTARS.2020.2971763>
- Lu, B., Dao, P. D., Liu, J., He, Y., & Shang, J. (2020). Recent advances of hyperspectral imaging technology and applications in agriculture. *Remote Sensing 2020*, Vol. 12, Page 2659, *12*(16), 2659. <https://doi.org/10.3390/RS12162659>
- Lu, T., Wan, L., & Wang, L. (2022). Fine crop classification in high resolution remote sensing based on deep learning. *Frontiers in Environmental Science*, *10*. <https://doi.org/10.3389/fenvs.2022.991173>
- Maponya, M. G., van Niekerk, A., & Mashimbye, Z. E. (2020). Pre-harvest classification of crop types using a Sentinel-2 time-series and machine learning. *Computers and Electronics in Agriculture*, *169*. <https://doi.org/10.1016/j.compag.2019.105164>

- Mohammadi, S., Belgiu, M., & Stein, A. (2021). 3D fully convolutional neural networks with intersection over union loss for crop mapping from multi-temporal satellite images. *International Geoscience and Remote Sensing Symposium (IGARSS)*. <https://doi.org/10.1109/IGARSS47720.2021.9554573>
- Pal, M., & Foody, G. M. (2010). Feature selection for classification of hyperspectral data by SVM. *IEEE Transactions on Geoscience and Remote Sensing*, 48(5). <https://doi.org/10.1109/TGRS.2009.2039484>
- Piedelobo, L., Hernández-López, D., Ballesteros, R., Chakhar, A., Del Pozo, S., González-Aguilera, D., & Moreno, M. A. (2019). Scalable pixel-based crop classification combining Sentinel-2 and Landsat-8 data time series: Case study of the Duero river basin. *Agricultural Systems*, 171. <https://doi.org/10.1016/j.agry.2019.01.005>
- Román, A., Heredia, S., Windle, A. E., Tovar-Sánchez, A., & Navarro, G. (2024). Enhancing georeferencing and mosaicking techniques over water surfaces with high-resolution unmanned aerial vehicle (UAV) imagery. *Remote Sensing*, 16(2). <https://doi.org/10.3390/rs16020290>
- Scheffler, D., Hollstein, A., Diedrich, H., Segl, K., & Hostert, P. (2017). AROSICS: An automated and robust open-source image co-registration software for multi-sensor satellite data. *Remote Sensing*, 9(7). <https://doi.org/10.3390/rs9070676>
- Schils, R. L. M., Bufe, C., Rhymer, C. M., Francksen, R. M., Klaus, V. H., Abdalla, M., Milazzo, F., Lellei-Kovács, E., Berge, H. ten, Bertora, C., Chodkiewicz, A., Dămătîrcă, C., Feigenwinter, I., Fernández-Rebollo, P., Ghiasi, S., Hejduk, S., Hiron, M., Janicka, M., Pellaton, R., ... Price, J. P. N. (2022). Permanent grasslands in Europe: Land use change and intensification decrease their multifunctionality. *Agriculture, Ecosystems and Environment*, 330. <https://doi.org/10.1016/j.agee.2022.107891>
- Seyrek, E. C., & Uysal, M. (2024). A comparative analysis of various activation functions and optimizers in a convolutional neural network for hyperspectral image classification. *Multimedia Tools and Applications*, 83(18). <https://doi.org/10.1007/s11042-023-17546-5>
- Shaik, R. U., Periasamy, S., & Zeng, W. (2023). Potential assessment of PRISMA hyperspectral imagery for remote sensing applications. *Remote Sensing*, 15(5). <https://doi.org/10.3390/rs15051378>
- Siesto, G., Fernández-Sellers, M., & Lozano-Tello, A. (2021). Crop classification of satellite imagery using synthetic multitemporal and multispectral images in convolutional neural networks. *Remote Sensing*, 13(17). <https://doi.org/10.3390/rs13173378>



- Skakun, S., Kussul, N., Shelestov, A. Y., Lavreniuk, M., & Kussul, O. (2016). Efficiency assessment of multitemporal C-Band Radarsat-2 intensity and Landsat-8 surface reflectance satellite imagery for crop classification in Ukraine. *IEEE Journal of Selected Topics in Applied Earth Observations and Remote Sensing*, 9(8). <https://doi.org/10.1109/JSTARS.2015.2454297>
- Spiller, D., Ansalone, L., Carotenuto, F., & Mathieu, P. P. (2021). Crop type mapping using PRISMA hyperspectral images and one-dimensional convolutional neural network. *International Geoscience and Remote Sensing Symposium (IGARSS)*, 8166–8169. <https://doi.org/10.1109/IGARSS47720.2021.9554175>
- Torbick, N., Huang, X., Ziniti, B., Johnson, D., Masek, J., & Reba, M. (2018). Fusion of moderate resolution earth observations for operational crop type mapping. *Remote Sensing*, 10(7), 1058. <https://doi.org/10.3390/RS10071058>
- United Nations. (2019). Population division world population prospects 2019. *World Population Prospects - 2019 Revision*.
- Vaddi, R., & Manoharan, P. (2020). Hyperspectral image classification using CNN with spectral and spatial features integration. *Infrared Physics and Technology*, 107. <https://doi.org/10.1016/j.infrared.2020.103296>
- van der Velde, M., & Nisini, L. (2019). Performance of the MARS-crop yield forecasting system for the European Union: Assessing accuracy, in-season, and year-to-year improvements from 1993 to 2015. *Agricultural Systems*, 168. <https://doi.org/10.1016/j.agry.2018.06.009>
- Vangi, E., D'amico, G., Francini, S., Giannetti, F., Lasserre, B., Marchetti, M., & Chirici, G. (2021). The new hyperspectral satellite prisma: Imagery for forest types discrimination. *Sensors (Switzerland)*, 21(4). <https://doi.org/10.3390/s21041182>
- Veloso, A., Mermoz, S., Bouvet, A., Le Toan, T., Planells, M., Dejoux, J. F., & Ceschia, E. (2017). Understanding the temporal behavior of crops using Sentinel-1 and Sentinel-2-like data for agricultural applications. *Remote Sensing of Environment*, 199. <https://doi.org/10.1016/j.rse.2017.07.015>
- Vuolo, F., Neuwirth, M., Immitzer, M., Atzberger, C., & Ng, W. T. (2018). How much does multi-temporal Sentinel-2 data improve crop type classification? *International Journal of Applied Earth Observation and Geoinformation*, 72. <https://doi.org/10.1016/j.jag.2018.06.007>

- Wang, X., Zhang, J., Xun, L., Wang, J., Wu, Z., HENCHIRI, M., Zhang, S., Zhang, S., Bai, Y., Yang, S., Li, S., & Yu, X. (2022). Evaluating the effectiveness of machine learning and deep learning models combined time-series satellite data for multiple crop types classification over a large-scale region. *Remote Sensing*, *14*(10). <https://doi.org/10.3390/rs14102341>
- Wang, Y., Feng, L., Zhang, Z., & Tian, F. (2023). An unsupervised domain adaptation deep learning method for spatial and temporal transferable crop type mapping using Sentinel-2 imagery. *ISPRS Journal of Photogrammetry and Remote Sensing*, *199*. <https://doi.org/10.1016/j.isprsjprs.2023.04.002>
- Whitcraft, A. K., Vermote, E. F., Becker-Reshef, I., & Justice, C. O. (2015). Cloud cover throughout the agricultural growing season: Impacts on passive optical earth observations. *Remote Sensing of Environment*, *156*. <https://doi.org/10.1016/j.rse.2014.10.009>
- Wiśniewska, A., Andryka-Dudek, P., Czerwiński, M., & Chołuj, D. (2019). Fodder beet is a reservoir of drought tolerance alleles for sugar beet breeding. *Plant Physiology and Biochemistry*, *145*. <https://doi.org/10.1016/j.plaphy.2019.10.031>
- Wu, B., Zhang, M., Zeng, H., Tian, F., Potgieter, A. B., Qin, X., Yan, N., Chang, S., Zhao, Y., Dong, Q., Boken, V., Plotnikov, D., Guo, H., Wu, F., Zhao, H., Deronde, B., Tits, L., & Loupian, E. (2023). Challenges and opportunities in remote sensing-based crop monitoring: a review. In *National Science Review* (Vol. 10, Issue 4). <https://doi.org/10.1093/nsr/nwac290>
- Xie, J., Hua, J., Chen, S., Wu, P., Gao, P., Sun, D., Lyu, Z., Lyu, S., Xue, X., & Lu, J. (2023). HyperSFormer: A Transformer-based end-to-end hyperspectral image classification method for crop classification. *Remote Sensing*, *15*(14). <https://doi.org/10.3390/rs15143491>
- Yi, Z., Jia, L., & Chen, Q. (2020). Crop classification using multi-temporal sentinel-2 data in the Shiyang river basin of China. *Remote Sensing*, *12*(24). <https://doi.org/10.3390/rs12244052>
- Zafar, A., Aamir, M., Mohd Nawi, N., Arshad, A., Riaz, S., Alruban, A., Dutta, A. K., & Almotairi, S. (2022). A comparison of pooling methods for convolutional neural networks. In *Applied Sciences (Switzerland)* (Vol. 12, Issue 17). <https://doi.org/10.3390/app12178643>
- Zhang, H., Kang, J., Xu, X., & Zhang, L. (2020). Accessing the temporal and spectral features in crop type mapping using multi-temporal Sentinel-2 imagery: A case study of Yi'an

- County, Heilongjiang province, China. *Computers and Electronics in Agriculture*, 176. <https://doi.org/10.1016/j.compag.2020.105618>
- Zhao, H., Chen, Z., Jiang, H., Jing, W., Sun, L., & Feng, M. (2019). Evaluation of three deep learning models for early crop classification using Sentinel-1A imagery time series-a case study in Zhanjiang, China. *Remote Sensing*, 11(22). <https://doi.org/10.3390/rs11222673>
- Zhao, Y., Liu, Z., & Wu, J. (2020). Grassland ecosystem services: a systematic review of research advances and future directions. *Landscape Ecology*, 35(4). <https://doi.org/10.1007/s10980-020-00980-3>
- Zhong, L., Hu, L., & Zhou, H. (2019). Deep learning based multi-temporal crop classification. *Remote Sensing of Environment*, 221. <https://doi.org/10.1016/j.rse.2018.11.032>

# ANNEX 1. WAVELENGTH RANGE OF MERGING BANDS ON PRISMA IMAGERY

Merge Bands			Near-Infrared (VNIR) Bands			Short-Wave Infrared (SWIR) Bands		
Band	Min Wavelength	Max Wavelength	Band	Min Wavelength	Max Wavelength	Band	Min Wavelength	Max Wavelength
1	402,57	411,42	1	402,57	411,42			
2	411,42	419,81	2	411,42	419,81			
3	419,81	427,56	3	419,81	427,56			
4	427,56	435,00	4	427,56	435,00			
5	435,00	442,34	5	435,00	442,34			
6	442,34	449,70	6	442,34	449,70			
7	449,70	457,06	7	449,70	457,06			
8	457,06	464,42	8	457,06	464,42			
9	464,42	471,71	9	464,42	471,71			
10	471,71	478,93	10	471,71	478,93			
11	478,93	486,17	11	478,93	486,17			
12	486,17	493,43	12	486,17	493,43			
13	493,43	500,79	13	493,43	500,79			
14	500,79	508,28	14	500,79	508,28			
15	508,28	515,80	15	508,28	515,80			
16	515,80	523,42	16	515,80	523,42			
17	523,42	531,18	17	523,42	531,18			
18	531,18	538,97	18	531,18	538,97			
19	538,97	546,90	19	538,97	546,90			
20	546,90	554,97	20	546,90	554,97			
21	554,97	563,11	21	554,97	563,11			
22	563,11	571,35	22	563,11	571,35			
23	571,35	579,67	23	571,35	579,67			
24	579,67	588,09	24	579,67	588,09			
25	588,09	596,68	25	588,09	596,68			
26	596,68	605,49	26	596,68	605,49			
27	605,49	614,34	27	605,49	614,34			
28	614,34	623,25	28	614,34	623,25			
29	623,25	632,23	29	623,25	632,23			
30	632,23	641,32	30	632,23	641,32			
31	641,32	650,69	31	641,32	650,69			
32	650,69	660,16	32	650,69	660,16			
33	660,16	669,68	33	660,16	669,68			
34	669,68	679,30	34	669,68	679,30			
35	679,30	689,13	35	679,30	689,13			
36	689,13	698,93	36	689,13	698,93			
37	698,93	708,73	37	698,93	708,73			

38	708,73	718,80	38	708,73	718,80			
39	718,80	728,92	39	718,80	728,92			
40	728,92	739,05	40	728,92	739,05			
41	739,05	749,31	41	739,05	749,31			
42	749,31	759,66	42	749,31	759,66			
43	759,66	770,06	43	759,66	770,06			
44	770,06	780,47	44	770,06	780,47			
45	780,47	790,89	45	780,47	790,89			
46	790,89	801,42	46	790,89	801,42			
47	801,42	812,01	47	801,42	812,01			
48	812,01	822,62	48	812,01	822,62			
49	822,62	833,22	49	822,62	833,22			
50	833,22	843,87	50	833,22	843,87			
51	843,87	854,59	51	843,87	854,59			
52	854,59	865,36	52	854,59	865,36			
53	865,36	876,10	53	865,36	876,10			
54	876,10	886,77	54	876,10	886,77			
55	886,77	897,44	55	886,77	897,44			
56	897,44	908,12	56	897,44	908,12			
57	908,12	918,70	57	908,12	918,70			
58	918,70	929,03	58	918,70	929,03			
59	929,03	938,73	59	929,03	939,37			
60	938,73	947,38	60	939,37	950,45	3	939,34	947,38
61	947,38	955,69	61	950,45	961,65	4	947,38	955,69
62	955,69	964,91	62	961,65	972,20	5	955,69	964,91
63	964,91	974,53	63	972,20	982,53	6	964,91	974,53
64	974,53	984,07				7	974,53	984,07
65	984,07	993,91				8	984,07	993,91
66	993,91	1003,78				9	993,91	1003,78
67	1003,78	1013,59				10	1003,78	1013,59
68	1013,59	1023,94				11	1013,59	1023,94
69	1023,94	1033,67				12	1023,94	1033,67
70	1033,67	1042,83				13	1033,67	1042,83
71	1042,83	1052,62				14	1042,83	1052,62
72	1052,62	1062,68				15	1052,62	1062,68
73	1062,68	1073,01				16	1062,68	1073,01
74	1073,01	1083,49				17	1073,01	1083,49
75	1083,49	1094,02				18	1083,49	1094,02
76	1094,02	1104,58				19	1094,02	1104,58
77	1104,58	1115,28				20	1104,58	1115,28
78	1115,28	1125,99				21	1115,28	1125,99
79	1125,99	1136,69				22	1125,99	1136,69
80	1136,69	1147,36				23	1136,69	1147,36
81	1147,36	1158,16				24	1147,36	1158,16
82	1158,16	1169,20				25	1158,16	1169,20

83	1169,20	1180,15				26	1169,20	1180,15
84	1180,15	1190,96				27	1180,15	1190,96
85	1190,96	1201,81				28	1190,96	1201,81
86	1201,81	1212,57				29	1201,81	1212,57
87	1212,57	1223,52				30	1212,57	1223,52
88	1223,52	1234,70				31	1223,52	1234,70
89	1234,70	1245,60				32	1234,70	1245,60
90	1245,60	1256,76				33	1245,60	1256,76
91	1256,76	1268,01				34	1256,76	1268,01
92	1268,01	1278,99				35	1268,01	1278,99
93	1278,99	1289,95				36	1278,99	1289,95
94	1289,95	1300,82				37	1289,95	1300,82
95	1300,82	1311,74				38	1300,82	1311,74
96	1311,74	1322,78				39	1311,74	1322,78
97	1322,78	1333,71				40	1322,78	1333,71
98	1333,71	1344,46				41	1333,71	1344,46
99	1344,46	1355,42				42	1344,46	1355,42
100	1355,42	1366,98				43	1355,42	1366,98
101	1366,98	1378,10				44	1366,98	1378,10
102	1378,10	1389,02				45	1378,10	1389,02
103	1389,02	1400,19				46	1389,02	1400,19
104	1400,19	1411,08				47	1400,19	1411,08
105	1411,08	1421,96				48	1411,08	1421,96
106	1421,96	1432,92				49	1421,96	1432,92
107	1432,92	1443,83				50	1432,92	1443,83
108	1443,83	1454,25				51	1443,83	1454,25
109	1454,25	1464,62				52	1454,25	1464,62
110	1464,62	1475,39				53	1464,62	1475,39
111	1475,39	1486,14				54	1475,39	1486,14
112	1486,14	1496,73				55	1486,14	1496,73
113	1496,73	1507,33				56	1496,73	1507,33
114	1507,33	1517,93				57	1507,33	1517,93
115	1517,93	1528,50				58	1517,93	1528,50
116	1528,50	1539,00				59	1528,50	1539,00
117	1539,00	1549,52				60	1539,00	1549,52
118	1549,52	1560,09				61	1549,52	1560,09
119	1560,09	1570,50				62	1560,09	1570,50
120	1570,50	1580,74				63	1570,50	1580,74
121	1580,74	1591,05				64	1580,74	1591,05
122	1591,05	1601,37				65	1591,05	1601,37
123	1601,37	1611,66				66	1601,37	1611,66
124	1611,66	1621,93				67	1611,66	1621,93
125	1621,93	1632,06				68	1621,93	1632,06
126	1632,06	1642,16				69	1632,06	1642,16
127	1642,16	1652,08				70	1642,16	1652,08

128	1652,08	1662,06				71	1652,08	1662,06
129	1662,06	1672,25				72	1662,06	1672,25
130	1672,25	1682,37				73	1672,25	1682,37
131	1682,37	1692,36				74	1682,37	1692,36
132	1692,36	1702,19				75	1692,36	1702,19
133	1702,19	1711,98				76	1702,19	1711,98
134	1711,98	1721,76				77	1711,98	1721,76
135	1721,76	1731,57				78	1721,76	1731,57
136	1731,57	1741,35				79	1731,57	1741,35
137	1741,35	1751,03				80	1741,35	1751,03
138	1751,03	1760,67				81	1751,03	1760,67
139	1760,67	1770,32				82	1760,67	1770,32
140	1770,32	1779,92				83	1770,32	1779,92
141	1779,92	1789,34				84	1779,92	1789,34
142	1789,34	1798,77				85	1789,34	1798,77
143	1798,77	1808,32				86	1798,77	1808,32
144	1808,32	1817,75				87	1808,32	1817,75
145	1817,75	1827,23				88	1817,75	1827,23
146	1827,23	1836,68				89	1827,23	1836,68
147	1836,68	1845,94				90	1836,68	1845,94
148	1845,94	1855,06				91	1845,94	1855,06
149	1855,06	1863,87				92	1855,06	1863,87
150	1863,87	1873,46				93	1863,87	1873,46
151	1873,46	1882,91				94	1873,46	1882,91
152	1882,91	1891,59				95	1882,91	1891,59
153	1891,59	1900,51				96	1891,59	1900,51
154	1900,51	1909,62				97	1900,51	1909,62
155	1909,62	1918,84				98	1909,62	1918,84
156	1918,84	1927,82				99	1918,84	1927,82
157	1927,82	1936,69				100	1927,82	1936,69
158	1936,69	1945,51				101	1936,69	1945,51
159	1945,51	1954,26				102	1945,51	1954,26
160	1954,26	1962,98				103	1954,26	1962,98
161	1962,98	1971,68				104	1962,98	1971,68
162	1971,68	1980,43				105	1971,68	1980,43
163	1980,43	1989,20				106	1980,43	1989,20
164	1989,20	1997,83				107	1989,20	1997,83
165	1997,83	2006,39				108	1997,83	2006,39
166	2006,39	2014,99				109	2006,39	2014,99
167	2014,99	2023,52				110	2014,99	2023,52
168	2023,52	2031,99				111	2023,52	2031,99
169	2031,99	2040,47				112	2031,99	2040,47
170	2040,47	2048,84				113	2040,47	2048,84
171	2048,84	2057,19				114	2048,84	2057,19
172	2057,19	2065,59				115	2057,19	2065,59

173	2065,59	2073,89				116	2065,59	2073,89
174	2073,89	2082,19				117	2073,89	2082,19
175	2082,19	2090,50				118	2082,19	2090,50
176	2090,50	2098,72				119	2090,50	2098,72
177	2098,72	2106,93				120	2098,72	2106,93
178	2106,93	2115,14				121	2106,93	2115,14
179	2115,14	2123,28				122	2115,14	2123,28
180	2123,28	2131,42				123	2123,28	2131,42
181	2131,42	2139,49				124	2131,42	2139,49
182	2139,49	2147,43				125	2139,49	2147,43
183	2147,43	2155,48				126	2147,43	2155,48
184	2155,48	2163,52				127	2155,48	2163,52
185	2163,52	2171,41				128	2163,52	2171,41
186	2171,41	2179,38				129	2171,41	2179,38
187	2179,38	2187,26				130	2179,38	2187,26
188	2187,26	2195,12				131	2187,26	2195,12
189	2195,12	2202,99				132	2195,12	2202,99
190	2202,99	2210,73				133	2202,99	2210,73
191	2210,73	2218,53				134	2210,73	2218,53
192	2218,53	2226,22				135	2218,53	2226,22
193	2226,22	2233,96				136	2226,22	2233,96
194	2233,96	2241,68				137	2233,96	2241,68
195	2241,68	2249,28				138	2241,68	2249,28
196	2249,28	2256,99				139	2249,28	2256,99
197	2256,99	2264,58				140	2256,99	2264,58
198	2264,58	2272,17				141	2264,58	2272,17
199	2272,17	2279,77				142	2272,17	2279,77
200	2279,77	2287,16				143	2279,77	2287,16
201	2287,16	2294,72				144	2287,16	2294,72
202	2294,72	2302,17				145	2294,72	2302,17
203	2302,17	2309,46				146	2302,17	2309,46
204	2309,46	2317,05				147	2309,46	2317,05
205	2317,05	2324,36				148	2317,05	2324,36
206	2324,36	2331,68				149	2324,36	2331,68
207	2331,68	2339,17				150	2331,68	2339,17
208	2339,17	2346,31				151	2339,17	2346,31
209	2346,31	2353,54				152	2346,31	2353,54
210	2353,54	2360,94				153	2353,54	2360,94
211	2360,94	2368,07				154	2360,94	2368,07
212	2368,07	2375,16				155	2368,07	2375,16
213	2375,16	2382,42				156	2375,16	2382,42
214	2382,42	2389,55				157	2382,42	2389,55
215	2389,55	2396,54				158	2389,55	2396,54
216	2396,54	2403,82				159	2396,54	2403,82
217	2403,82	2410,98				160	2403,82	2410,98



<b>218</b>	2410,98	2417,80				<b>161</b>	2410,98	2417,80
<b>219</b>	2417,80	2424,95				<b>162</b>	2417,80	2424,95
<b>220</b>	2424,95	2432,11				<b>163</b>	2424,95	2432,11
<b>221</b>	2432,11	2438,97				<b>164</b>	2432,11	2438,97
<b>222</b>	2438,97	2445,77				<b>165</b>	2438,97	2445,77
<b>223</b>	2445,77	2452,86				<b>166</b>	2445,77	2452,86
<b>224</b>	2452,86	2459,81				<b>167</b>	2452,86	2459,81
<b>225</b>	2459,81	2466,33				<b>168</b>	2459,81	2466,33
<b>226</b>	2466,33	2473,34				<b>169</b>	2466,33	2473,34
<b>227</b>	2473,34	2480,42				<b>170</b>	2473,34	2480,42
<b>228</b>	2480,42	2487,01				<b>171</b>	2480,42	2487,01
<b>229</b>	2487,01	2493,67				<b>172</b>	2487,01	2493,67
<b>230</b>	2493,67	2500,56				<b>173</b>	2493,67	2500,56